

11-85

PL File
Universities

7N-07

P-52

Semi-Annual Report

11707

Heat Transfer and pressure Drop in Blade Cooling
Channels with Turbulence Promoters

by

J. C. Han

Texas A&M University
College Station, Texas

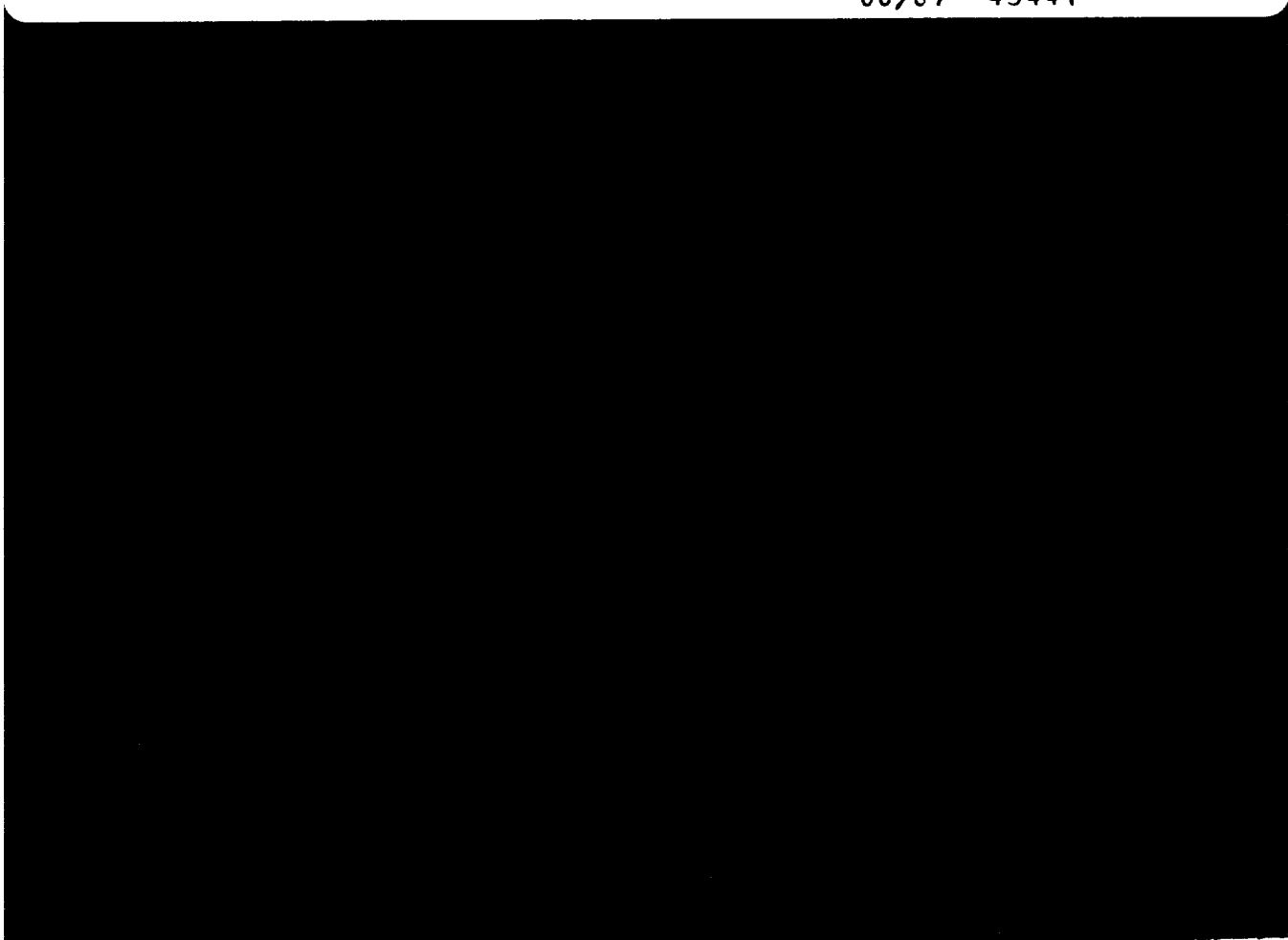
(NASA-CR-177209) HEAT TRANSFER AND PRESSURE
DROP IN BLADE COOLING CHANNELS WITH
TURBULENCE PROMOTERS Semiannual Report
(Texas A&M Univ.) 52 p

N86-72108

11707

Unclas

00/07 43441



C. Han
2/3/83

TEXAS A&M UNIVERSITY
MECHANICAL ENGINEERING DEPARTMENT

COLLEGE STATION, TEXAS 77843-3123

February 3, 1983

Mr. Curt Walker
Chief, Engines & HTC Div.
Mail Box 302-2
Propulsion Laboratory
NASA Lewis Research Center
21000 Brook Park Road
Cleveland, Ohio 44135

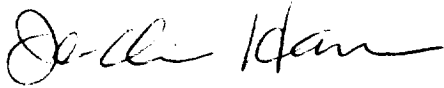
Dear Mr. Walker:

Enclosed please find two copies of the semi-annual report of our project entitled, "Heat Transfer and Pressure Drop in Blade Cooling Channels with Turbulence Promoters" sponsored by the U.S. Army Research and Technology Laboratory under NASA Grant NAG 3-311, for your review.

I am going to send two copies of the report to Mr. Boyle and Dr. Simoneau of NASA for their review also. The final report of the first phase project will be submitted before the end of July 1983.

We appreciate your support very much. We also thank Mr. Boyle for monitoring the project.

With best wishes,



J. C. Han
Assistant Professor

cc: Mr. R. J. Boyle
Dr. R. J. Simoneau

Semi-Annual Report

Heat Transfer and pressure Drop in Blade Cooling
Channels with Turbulence Promoters

by

J. C. Han

Texas A&M University
College Station, Texas

Prepared for

The U.S. Army Research and Technology Laboratory
Under NASA Grant NAG3-311

January 1983

Contents

	Page
Nomenclature -----	iii
Summary -----	1
I. Introduction -----	4
II. The Experimental Apparatus -----	7
II-A. Long Duct Entrance -----	7
II-B. Sudden Contraction Entrance -----	9
III. Analysis of Data -----	11
III-A. Long Duct Entrance -----	11
III-B. Sudden Contraction Entrance -----	13
IV. Experimental Results -----	14
IV-A. Long Duct Entrance -----	14
IV-B. Sudden Contraction Entrance -----	16
Reference -----	18
Figures -----	20
Photographs -----	45

Nomenclature

D	side to side dimension of square duct
D_e	equivalent diameter - four times the cross-sectional area divided by the wetted perimeter; $D_e = D$ for square duct
e	rib height
e^+	roughness Reynolds number $(e/D_e) Re (f/2)^{1/2}$
f	friction factor, see equation (1)
g_c	conversion factor, see equation (1)
G	mass flux ρV_m
h	heat transfer coefficient
K	thermal conductivity of fluid
L	the distance between the centerline and the edge of the duct; $L = \frac{1}{2} D$
L	test section length for friction pressure drop
\bar{N}_u	spanwise-average Nusselt number, see equations (2) and (3)
N_u	local Nusselt number, see equations (4) and (5)
N_{ufs}	Nusselt number of four sided smooth surfaces
Δp	pressure drop across the test section
p	rib pitch
Pr	Prandtl number of fluid
q''	heat transfer rate per unit time per unit surface area
Re	Reynolds number GD_e/μ
St	Stanton number $Nu/(Re Pr)$
T	temperature
T_b	bulk mean temperature of fluid
T_w	temperature at the wall
V_m	average velocity of fluid
X	the axial distance from the heated test duct

z the lateral distance from the centerline of the duct
 α flow attack angle
 ρ average density of fluid
 μ average viscosity of fluid
 η efficiency index of the rough duct $(S_{tr}/S_{ts})/(f_r/f_s)$

Subscripts

f_s four sided smooth surfaces
 s smooth side wall
 r ribbed side wall
 D parameters based on the side-to-side dimension of square duct

Summary

This is the semi-annual report for the program of Heat Transfer and Pressure Drop in Blade Cooling Channels with Turbulence Promoters. This project is conducted by the Texas A&M University and is funded by the U.S. Army Research and Technology Laboratory. The project is monitored by the NASA-Lewis Research Center under NASA Grant No. NAG 3-311.

In advanced turbine blade cooling design, the 90° ribs have been casted onto the surfaces of the cooling ducts in order to enhance the heat transfer capability. The objective of the project was to investigate the effect of rib angle-of-attack on the pressure drop and the average heat transfer coefficients in a square duct with two opposite ribbed walls for Reynolds number varied from 10^4 to 10^5 . The rib angle-of-attack (α) was varied from 90° to 60° to 45° to 30° , respectively; whereas the rib pitch-to-height ratio ($p/e = 10$) and the rib height-to-equivalent diameter ratio ($e/D_e = 0.063$) were kept at constant in all tests. Two types of entrance conditions were examined, namely, long duct and sudden contraction, respectively. The local heat transfer coefficient distributions on the smooth side wall and between the ribs of the rough side wall at the entrance and the fully developed regions were measured.

The program consisted of the following tasks:

Task I - study the effect of rib angle-of-attack on the friction factor and the spanwise-average heat transfer coefficients in the fully developed region for the case of long duct entrance.

I-A. Construction of the test apparatus - An aluminum square duct with 3" x 3" cross section.

I-B. Tests on the square duct with four sided smooth walls.

I-C. Tests on the same square duct with two opposite ribbed walls with $\alpha = 90^\circ$.

I-D. Tests on the same square duct with $\alpha = 45^\circ$.

I-E. Tests on the same square duct with $\alpha = 30^\circ$

I-F. Tests on the same square duct with $\alpha = 60^\circ$

Task II - study the effect of rib angle-of-attack on the friction factor and the local heat transfer coefficient distributions on the smooth side wall and between the ribs of the rough side wall at the entrance and the fully developed regions for the case of sudden contraction entrance.

II-A. Construction of the test apparatus - A stainless steel square duct with 3" x 3" cross section.

II-B. Tests on the square duct with four sided smooth walls.

II-C. Tests on the same square duct with two opposite ribbed walls with $\alpha = 90^\circ$

II-D. Tests on the same square duct with $\alpha = 45^\circ$

II-E. Test on the same square duct with $\alpha = 30^\circ$

II-F. Tests on the same square duct with $\alpha = 15^\circ$

Task III - Development of the semi-analytical correlations for friction factor and heat transfer coefficients in square ducts with two opposite rib-roughened walls for the different rib flow-attack-angles. Identification of the best rib angle-of-attack for the blade internal cooling design.

This progress report covers the data have been obtained for the Tasks I-A to I-E and II-A to II-C. The results of Tasks I-B and II-B showed that the friction and heat transfer data for flow in the square duct with four sided smooth walls agreed well with the results given in the literature. The results of Tasks I-C and II-C ($\alpha = 90^\circ$) showed that the heat transfer coefficients of the ribbed side wall was about 2-3 times that of the four sided smooth duct and the heat transfer coefficients of the smooth side wall was also enhanced by 40-60% due to the presence of the ribs on the adjacent walls; whereas the

friction factor was increased about 4-6 times. The results of Task I-D ($\alpha = 45^\circ$) showed that the ribbed side heat transfer coefficients was higher than that of $\alpha = 90^\circ$ by 5-10%; while the friction factor was lower by 5%. However, the results of Task I-E ($\alpha = 30^\circ$) showed that the ribbed side heat transfer coefficients was lower than $\alpha = 90^\circ$ by 10-15%; whereas the friction factor was lower by 30-40%. It suggests that the best thermal performance is obtained with the 30° rib angle-of-attack. It should be noted that the best performance angle was reported with the 45° rib angle-of-attack for flow between parallel-plates and in tubes (i.e., four sided ribbed duct) by the previous investigations [6-7].

The local heat transfer coefficient distribution on the smooth side wall and between the ribs of the rough side wall at the entrance and the fully developed regions were obtained from the results of Task II-C ($\alpha = 90^\circ$). It showed that the ribbed side wall had a much higher augmentation than the smooth side wall; whereas the edgeline region had a little bit higher enhancement than the centerline region of the duct. It also indicated that the lateral heat transfer coefficient had a lower value somewhere between the ribs and reached the maximum at the rib tip. The heat transfer coefficient variations between the ribs were more pronounced by increasing the Reynolds number.

After completion of Task III by the end of July, 1983, a final report will be submitted.

I. Introduction

One of the well known methods to enhance the heat transfer from a surface is to roughen the surface by the use of two-dimensional repeated-ribs on the surface. However, the increase in heat transfer is accompanied by an increase in the pressure drop of the fluid flow. Many investigations have been directed toward developing predictive correlations for a given rib geometry and establishing a geometry which gives the best heat transfer performance for a given pumping power.

Fully developed turbulent heat transfer and friction in tubes with repeated-rib rougheners have been studied extensively [1-7]. Considerable data also exists for repeated-rib-roughness in an annular flow geometry in which the inner annular surface is rough and the outer surface is smooth to simulate the geometry of fuel bundles in advanced gas-cooled nuclear reactor [8-12]. Based on those previous studies, the effects of rib height-to-equivalent diameter ratio, e/D_e , and rib pitch-to-height ratio, P/e , on the heat transfer coefficients and friction factor over a wide range of Reynolds number are well established. Recently, Han et al. [6] used a parallel-plate channel geometry to study the effect of rib height-to-equivalent diameter ratio, rib pitch-to-height ratio, and rib angle-of-attack (See Fig. 1). They concluded that a 45° angle-of-attack provided superior performance at a given friction power when compared to ribs at a 90° angle-of-attack. The similar results had been reported by Gee and Webb [7] who conducted forced convection heat transfer in helically rib-roughened tubes. However, in some applications, such as turbine blade internal cooling design, the enhanced heat transfer capability is desired on only two opposite walls of a rectangular duct [13-15]. The heat transfer and friction characteristics in channels of this kind may be different from those of circular tubes, parallel-plates, or Annuli. The only available data was reported by Burggraf [16] who studied the square duct with two opposite

rib-roughened walls with a rib flow-attack-angle of 90° , rib pitch-to-height ratio of 10, and rib height-to-equivalent diameter ratio of 0.055. Air was the working fluid; constant wall temperature was the boundary condition. Three types of entrance conditions were tested over Reynolds numbers (Re_D) from 1.3×10^4 to 1.3×10^5 , namely, downstream of a fully developed hydrodynamic flow (long duct entrance), downstream of a rounded entrance from a plenum (short duct entrance), and downstream of a 180° bend, respectively. For the long duct entrance case, Burggraf found the augmentation of the Nusselt number on the ribbed side wall was 2.38 times the fully developed smooth duct flow values when the characteristic dimension was taken as twice the plate spacing. The augmentation of the friction factor was approximately 8.6 times that of the smooth duct results. There was also enhancement of the smooth side wall heat transfer by 19% over the all smooth correlations. He also reported similar trends for the case of a short duct entrance and for the 180° bend tests. In this study the emphasis was placed on the effect of entrance conditions on the heat transfer coefficients. Only one particular rib angle-of-attack (i.e., $\alpha = 90^\circ$) was tested. Since then, no study has been reported to optimize the rib angle-of-attack in the blade cooling channels in order to obtain the best heat transfer performance for a given flow pressure drop. No further study to investigate the effect of channel aspect ratio on the heat transfer and friction can be found in the open literature. Moreover, the data of the local heat transfer coefficient distributions on the smooth side wall and between the ribs of the rough side wall are lacking. Therefore, basic research in this area is warrentable.

The objective of the project was to investigate the effect of rib angle-of-attack on the friction factor and the average heat transfer coefficients in a square duct with two opposite ribbed walls for Reynolds number varied from 10^4 to 10^5 . The rib angle-of-attack (α) was varied from 90° to 60° to 45° to

30°, respectively; whereas the rib pitch-to-height ratio ($p/e = 10$) and the rib height-to-equivalent diameter ratio ($e/D_e = 0.063$) were kept at constant in all tests. Two types of entrance conditions were examined, namely, long duct and sudden contraction, respectively. The local heat transfer coefficient distributions on the smooth side wall and between the ribs of the rough side wall at the entrance and the fully developed regions were measured. The second phase (second year) of the project will investigate the effect of rectangular duct aspect ratio on the friction factor and the heat transfer coefficients for the ribs at different angle-of-attack.

II. The Experimental Apparatus

II-A. Long Duct Entrance

The construction of the apparatus with a long duct entrance was completed before this project started on August, 1982. The purpose of this apparatus was to provide the friction factor and the average heat transfer coefficients data for flow in the fully developed region. Figure 2 shows a schematic of the test rig.

A blower forced air at room temperature and pressure through a 10.16 cm (4 in) diameter tube equipped with a 5.08 cm (2 in) diameter ASME square-edged orifice plate to measure flow rate. A transition section was used between the tube and the unheated entrance duct. At the end of the heated test duct, the air was exhausted into the atmosphere. The blower was capable of providing a range of air velocities so that the Reynolds number (ReD) in the test duct varied between 7,000 and 90,000.

The test duct which consisted of four heated parallel aluminum plates, 0.635 cm (0.25 in) thick, as shown in Figure 3, had cross-sectional dimensions 7.6 cm by 7.6 cm (3 in by 3 in) and a heated length of 20 duct diameters. The duct orientation was such that the two opposite rib-roughened walls of the square cross section were vertical and the two opposite smooth walls horizontal. These ribbed walls were made by gluing square brass ribs to the plate surface in a required distribution. The ribs serve as turbulence promoters to trip the laminar sublayer of the turbulent flow. For a glue thickness of 0.0127 cm (0.005 in.) or less, the heat transfer flux to the portion of the plate under the rib is reduced by less than 3%; thus the thermal resistance of the glue is negligible. A 0.159 cm (0.0625 in) thick asbestos strip was placed along the contact surface between the smooth and the ribbed walls to reduce the possible heat conduction effect. Woven heaters embedded in silicone rubber were adhered uniformly between the aluminum plate and a wood panel to insure good contact.

Each aluminum plate had one woven heater; each heater could be independently controlled by a variac transformer and provided a controllable constant heat flux for the entire test plate. The entire heated test duct, including unheated end duct, was mounted centrally in a long horizontal enclosure of cross-sectional dimensions 30.5 cm by 30.5 cm (12 in by 12 in). The enclosure was filled with fiber-glass insulating material. The unheated entrance duct had the same cross-section and length as those of the test duct although the entrance duct was made of plexi-glass plates. This entrance duct served to establish hydrodynamically fully developed flow at the entrance to the heated duct. Additionally, the entrance duct was ribbed over its length on two opposite walls in the same way as the test duct. The test section was instrumented with 36 thermocouples distributed along the length and across the span of the aluminum plates, as shown in Figure 4. Thermocouples were also used to measure the bulk mean air temperature entering and leaving the test section. Five pressure taps along the test duct (three on the smooth side and two on the ribbed side) were used for the static pressure drop measurements across the test duct.

II-B. Sudden Contraction Entrance

The construction of the apparatus with a sudden contraction entrance was completed by November, 1982. The purpose of this apparatus was to provide data of the pressure drop and the local heat transfer coefficients on the smooth side wall and between the ribs of the rough side wall for flow in the entrance and in the fully developed regions. Figure 5 shows a schematic of the test rig.

A 5 HP blower forced air through a 10.16 cm (4 in) diameter pipe equipped with a 3.8 cm (1.5 in) diameter orifice plate to measure flow rate. A plexi-glass plenum with a cross section of 38 cm by 38 cm (15 in by 15 in) and a length of 76 cm (30 in) was connected between the pipe and the test duct to ensure that the air entering the test duct was uniform and had a sudden contraction condition. The contraction ratio was 5:1. A round corner with a radius of 0.63 cm (0.25 in) was provided between the plenum and the test duct. The test section was designed to simulate the inlet condition of the cooling flow in the turbine blade. At the end of the test section, the air was exhausted into the atmosphere. The Reynolds number in the test duct was varied between 7×10^3 and 1.3×10^5 .

The test duct which consisted of four parallel stainless steel plates was constructed in the same way as that of the long duct entrance condition. The detail description of the test duct can be referred to paragraph II-A. The stainless steel plates were used to replace aluminum because of their low thermal conductivity, so that the local temperature distributions (therefore the local heat transfer coefficient distributions) on the smooth side wall and between the ribs of the rough side wall at the entrance and the fully developed regions could be measured. The test section was instrumented with 78 thermocouples distributed along the length and across the span of the stainless steel plates, as shown in Figure 6. Thermocouples were also used to measure the bulk mean air temperature entering and leaving the test duct. Six pressure

taps (two on the plenum and four on the test duct) were used for the static pressure drop measurements, as shown in Figure 7. The air flow, pressure drop, electrical heat input, and temperature measurements systems are shown in Figure 8.

III. Analysis of Data

III-A. Long Duct Entrance

The pressure drop across the test section was measured by a micro-manometer and checked by an inclined manometer. In fully developed duct flow, the friction factor can be determined by measuring the pressure drop across the flow channel and the mass flow rate of the air. The friction can be calculated from:

$$f = \frac{\Delta p}{4(L/D_e)(G^2/2\rho g_c)} \quad (1)$$

During the experiments, it was seen that the magnitude of the pressure drop was about the same when measured from the pressure taps on the smooth side or on the ribbed side wall. The maximum uncertainty in the friction factor was estimated to be 6.6% in this investigation.

For the longitudinally constant heat flux boundary condition of the present investigation, the thermally fully developed region is characterized by wall and fluid temperatures that increase linearly as a function of longitudinal position. The longitudinal distribution of the fluid bulk mean temperature was represented as a straight line connecting the measured values at inlet and exit. Typically, at downstream distances ranging from 10 to 15 hydraulic diameters from the start of heating, as shown in Figure 9, the wall temperature data paralleled the aforementioned bulk temperature straight line. Consequently, only those data corresponding to the thermally fully developed region were employed for the computation of the heat transfer coefficients. During the tests, it was found that the ribbed surface heat transfer capability was higher than that of the smooth surface. Consequently, the ribbed wall temperature was lower than the smooth one. In order to reduce the possible heat conduction effect between the smooth wall and the rough wall, the heat input to the smooth wall was controlled at about $\frac{2}{3}$

to $\frac{4}{5}$ that of the rough wall. Therefore the temperature difference between the adjacent walls was maintained between 0.6°C to 1.8°C (1°F to 3°F) in all tests, as seen in Figure 9. Additionally, in order to reduce the thermocouple inaccuracy, which strongly affects the calculated heat transfer coefficient, the temperature rise of air was maintained between 11°C and 17°C (20°F and 30°F), and the temperature difference between the wall and fluid was maintained between 22°C and 33°C (40°F and 50°F) in all tests.

The fully developed heat transfer coefficients to be reported here will be termed spanwise-average since they describe the average value of the full 7.6 cm (cross-sectional) span of the heated wall. The spanwise-average, fully developed Nusselt numbers, can be calculated from:

$$\bar{N}_{us} = \frac{q''_s}{(\overline{T_w - T_b})_s} \frac{D}{K} \quad (2)$$

and

$$\bar{N}_{ur} = \frac{q''_r}{(\overline{T_w - T_b})_r} \frac{D}{K} \quad (3)$$

The q''_s and q''_r represent the net heat flux from the smooth side and the ribbed side walls to the fluid, respectively, whereas $(\overline{T_w - T_b})_s$ and $(\overline{T_w - T_b})_r$ are the thermal driving forces averaged over the span of the smooth wall and the ribbed wall, respectively. Equation (2) was used for the smooth side wall average Nusselt number calculation while equation (3) was for the ribbed side wall. Notice that the ribbed side heat flux, q''_r , was based on the total heat transfer area including the rib surface area. The maximum uncertainty in the average Nusselt number was estimated to be 6.8% in this investigation.

III-B. Sudden Contraction Entrance

Equation (1) can be used to determine the friction factor for flow in the fully developed region. In heat transfer measurements, the local wall temperature distributions were measured by thermocouples. The heat transfer rate into the flow channel can be calculated either from Watts meters or from air flow enthalpy increase (air flow rate x specific heat x temperature increase). The bulk mean air temperature will be increased linearly through the test duct for the constant heat flux boundary condition of this experiments. Therefore, the local bulk mean air temperature can be calculated for the given heat input. Then the local Nusselt number can be determined by:

$$N_{us} = \frac{q''_s}{T_{ws} - T_b} \frac{D}{K} \quad (4)$$

$$N_{ur} = \frac{q''_r}{T_{wr} - T_b} \frac{D}{K} \quad (5)$$

The q''_s and q''_r represents the net constant heat flux from the smooth side and the ribbed side walls to the fluid, respectively; whereas T_{ws} and T_{wr} are the local wall temperatures on the smooth side and on the ribbed side, respectively. Equation (4) was used for the smooth side wall local heat transfer coefficient calculation while equation (5) was for the ribbed side wall.

IV. Experimental Results

IV-A. Long Duct Entrance

Before initiating experiments with rib-roughened walls, the friction factor and heat-transfer coefficient were measured for a smooth duct and compared with the results given in the literature, as shown in Figure 10. As seen by the figure there is good agreement between the accepted correlation [17] and the experimental results for the present smooth duct with 7.6 cm by 7.6 cm cross-section. The friction factor differs by about 5.5% from the tube flow results, and the Stanton number differs by about 6.5%. This proved that the apparatus was ready to reproduce data for flow in the same square duct with two opposite ribbed walls. The ribs had a square cross-section and were glued onto the surfaces at a certain angle to the direction of mainstream flow. The rib flow-attack-angle α was varied from 90° to 45° to 30° , respectively; whereas the rib pitch-to-height ratio ($p/e = 10$) and the rib height-to-equivalent diameter ratio ($e/D_e = 0.063$) were kept at the constant value in all tests. The friction factor vs Reynolds number for the different flow attack angles is shown in Figure 11. The friction factor of the ribbed duct with $\alpha = 90^\circ$ is about 4-6 times higher than that of the four sided smooth duct. For the $\alpha = 90^\circ$ and 45° , the friction factor approaches an approximately constant value as the Reynolds number increase; while the friction factor slightly decreases with Reynolds number when the $\alpha = 30^\circ$. It is seen that the friction factor only decreases by 5% when the rib flow-attack-angle changes from 90° to 45° , however, it decreases by 30 ~ 40% when the α changes from 90° to 30° . Figure 12 shows the spanwise-average Nusselt number of the ribbed side wall vs Reynolds number at different α . The Nusselt number (therefore the heat transfer coefficient) increases with increasing Reynolds number. The Nusselt number of the ribbed side wall with $\alpha = 90^\circ$ is about 2 times higher than that of the four sided smooth duct. The Nusselt number with $\alpha = 45^\circ$ is about 10% higher than that with $\alpha = 90^\circ$; whereas the

Nusselt number with $\alpha = 30^\circ$ is about 15% lower. As shown in Figure 13, the Nusselt number of the smooth side wall is also higher than that of the four sided smooth duct by 40-80% due to the presence of the ribs on the adjacent walls. Figure 14 shows the friction factor and Nusselt number vs the rib angle-of-attack. The data of the 0° angle-of-attack was obtained from the present smooth duct results. It is seen that the amount of the friction factor decrease is relatively larger than that of the Nusselt number when the rib angle-of-attack changes from 90° to 30° . This suggests that the best thermal performance may be obtained at the rib flow-attack-angle around 30° . Figure 15 shows the rough surface efficiency index (η) vs roughness Reynolds number (e^+). It is clearly seen that the best η is obtained with the 30° flow-attack-angle. It should be noted that the best performance angle was reported about 45° for flow between parallel-plates and in tubes (i.e., four sided ribbed duct) by the previous investigations [6-7]. Based on these observations, it may be concluded that the best operating angle is shifted from a 45° to a smaller angle (30°) when the square duct has only two opposite ribbed walls.

IV-B. Sudden Contraction Entrance

Before initiating experiments with ribbed walls, the pressure drop and heat transfer were calibrated for a four sided smooth duct and compared with the results given in the literature. Figure 16 shows the friction factor vs Reynolds number for flow in the fully developed region. The agreement between the accepted correlation and the present data is reasonably well. The plenum related pressure drop vs Reynolds number is plotted in Figure 17. The wall and the air bulk mean temperature distributions along the test section is shown in Figure 18 and Figure 19 for the Reynolds number $Re_D = 20,000$ and $83,000$, respectively. It is seen that the center line temperatures on the left hand side and the bottom walls are very close to each other. Figure 20 shows the Nusselt number for flow in the entrance length region at two different Reynolds numbers. Figure 21 shows the Nusselt number vs Reynolds number for flow in the fully developed region. The agreement between the existing correlation and the present data is acceptable. Based on these smooth duct results, the apparatus was ready to reproduce data for flow in the same duct with two opposite ribbed walls.

Figures 22-23 show the test results of the friction factor and Nusselt number for flow in the fully developed region with the rib $\alpha = 90^\circ$, $p/e = 10$, and $e/D_e = 0.063$. The increased friction factor and Nusselt number agree fairly well with that of Figures 11-13 as mentioned in the paragraph IV-A. The local Nusselt number augmentation on the smooth side wall and between the ribs of the rough side wall at the fully developed region is shown in Figure 24. It is expected that the ribbed side wall has a much higher enhancement than the smooth side wall. In general, the edge line region has a little bit higher enhancement than the centerline region of the duct. It also indicates that the Nusselt number augmentation decreases with increasing the Reynolds number. The lateral Nusselt number distribution between the ribs at the fully developed

region is shown in Figure 25. The Nusselt number has a lower value somewhere between the ribs and reaches the maximum at the rib tip. The Nusselt number variations between the ribs are more pronounced by increasing the Reynolds number.

References

1. Nunner, W., "Heat Transfer and Pressure Drop in Rough Tubes", AERE lib/Trans. 786, 1958.
2. Webb, R.L., Eckert, E.R.G., and Goldstein, R.J., "Heat Transfer and Friction in Tubes with Repeated-rib Roughness", Int. J. Heat Mass Transfer 14, 1971, pp. 601-617.
3. Lewis, M.J., "An Elementary Analysis for Predicting the Momentum and Heat Transfer Characteristics of a Hydraulically Rough Surface", J. Heat Transfer, Vol. 97, 1975, pp. 249-254.
4. Lewis, M.J., "Optimizing the Thermohydraulic Performance of Rough Surfaces", Int. J. Heat Mass Transfer, Vol. 18, 1975, pp. 1243-1248.
5. Kader, B.A. and Yaglom, a.M., "Turbulent Heat and Mass Transfer from a Wall with Parallel Roughness Ridges", Int. J. Heat Mass Transfer, Vol. 20, 1977, pp. 354-357.
6. Han, J.C., Glicksman, L.R., and Rohsenow, W.M., "An Investigation of Heat Transfer and Friction for Rib-Roughened Surfaces", Int. J. Heat Mass Transfer, Vol. 21, 1978, pp. 1143-1156, Also, Int. J. Heat Mass Transfer, Vol. 22, p. 1587, 1979.
7. Gee, D.L., and Webb, R.L., "Forced Convection Heat Transfer in Helically Rib-Roughened Tubes", Int. J. Heat Mass Transfer, Vol. 23, 1980, pp. 1127-1136.
8. Hall, W.B., "Heat Transfer in channels Having Rough and Smooth Surfaces", J. Mech. Enging. Sci. 4, 1962, pp. 287-291.
9. Wilkie, D. "Forced Convection Heat Transfer From Surfaces Roughened by Transverse Ribs", In proceedings of the 2nd Int. Heat Transfer Conference, Vol. 1, AICHE, New York, 1966.
10. White, L. and Wilkie, D., "The Heat Transfer and Pressure Loss Characteristics of Some Multi-start Ribbed Surfaces", In Augmentation of Convective Heat and Mass Transfer, edited by A.E. Bergles and R.L. Webb, ASME, New York, 1970.
11. Donne, D. and Meyer, L., "Turbulent Convective Heat Transfer From Rough Surfaces with Two-Dimensional Rectangular Ribs", Int. J. Heat Mass Transfer, Vol. 20, 1977, pp. 582-620.
12. Meyer, L., "Thermohydraulic Characteristics of Single Ribs with Three-Dimensional Roughness", Int. J. Heat Mass Transfer, Vol. 25, 1982, pp. 1043-1058.
13. Suo, M., "Turbine Cooling", In the Aerothermodynamics of Aircraft Gas Turbine Engines, Edited by Oates, G., Air Force Aero Propulsion Lab., AFAPL TR 78-52, 1978.

14. Hennecke, D.K., "Turbine Blade Cooling in Aero Engines-Some New Results, Future Trends, and Research Requirements", In study in Heat Transfer, edited by Hartnett et al., Hemisphere Corp., New York, 1979.
15. Taylor, J.R., "Heat Transfer Phenomena in Gas Turbine", ASME Paper No. 80-GT-172, 1980.
16. Burggraf, F., "Experimental Heat Transfer and Pressure Drop with Two-Dimensional Turbulence Promoter Applied to Two Opposite Walls of a Square Tube", In Augmentation of Convective Heat and Mass Transfer, edited by E.E. Bergles and R.L. Webb, ASME, New York, 1970, pp. 70-79.
17. Rohsenow, W.M., and Hartnett, J.P., "Handbook of Heat Transfer", McGraw-Hill, Inc., New York, 1973.

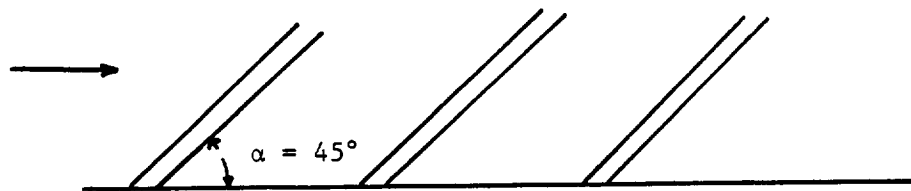
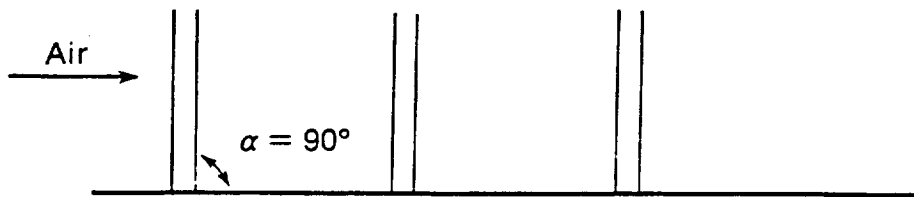
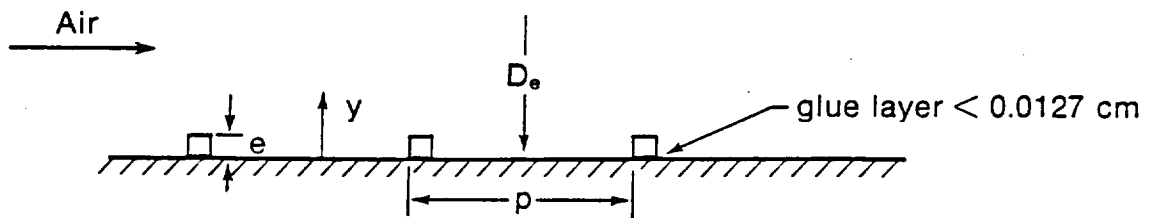


Figure 1. Rib geometry

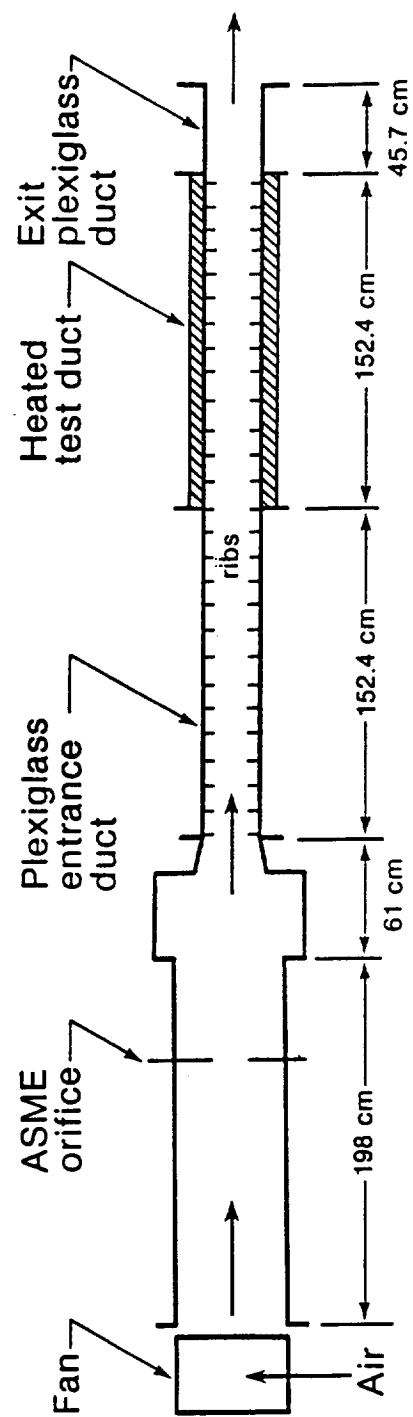


Figure 2. Top view of the experimental apparatus

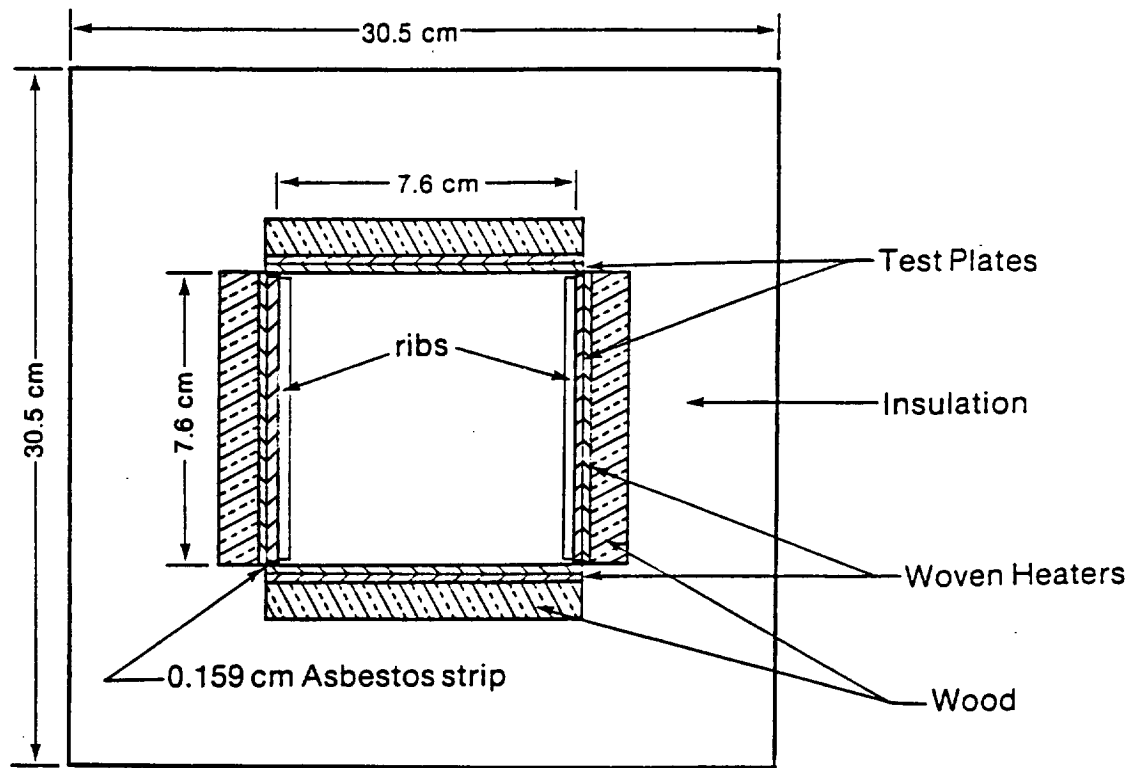


Figure 3. Cross-section of test duct

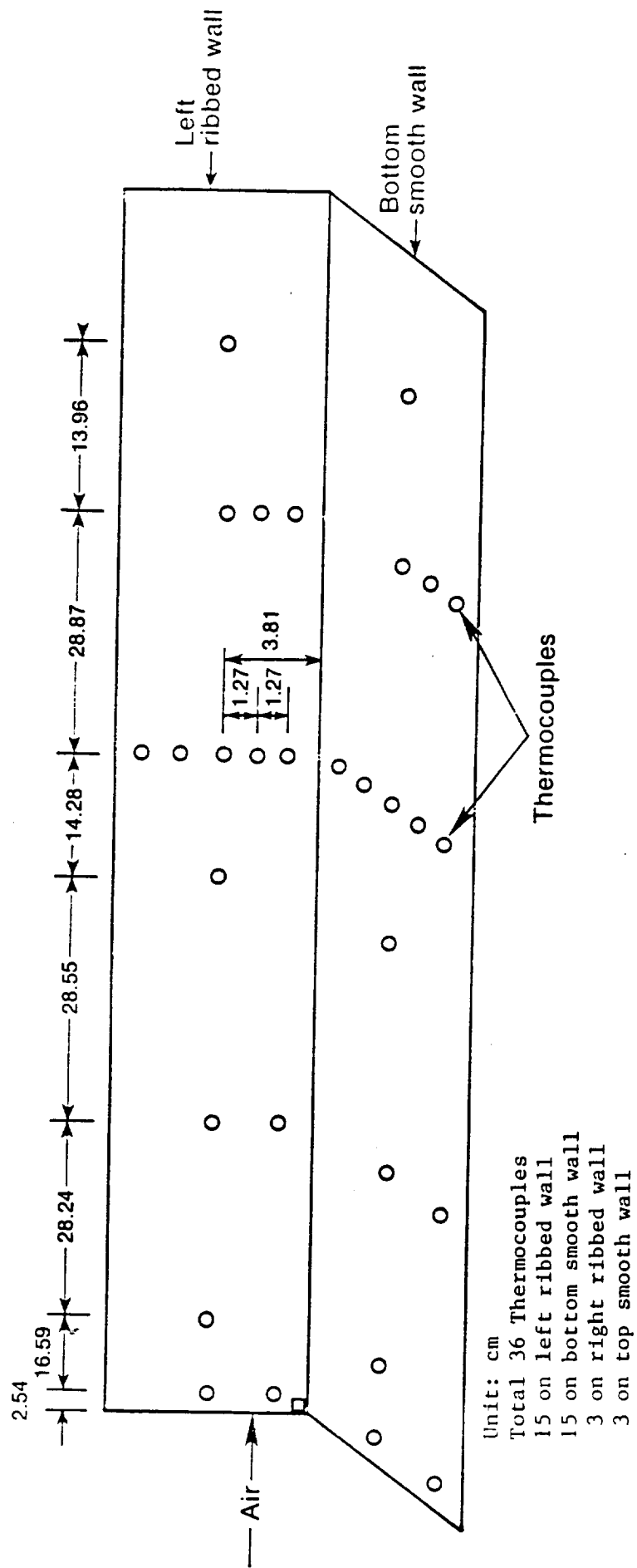


Figure 4. Detail of thermocouples distributions on test plates

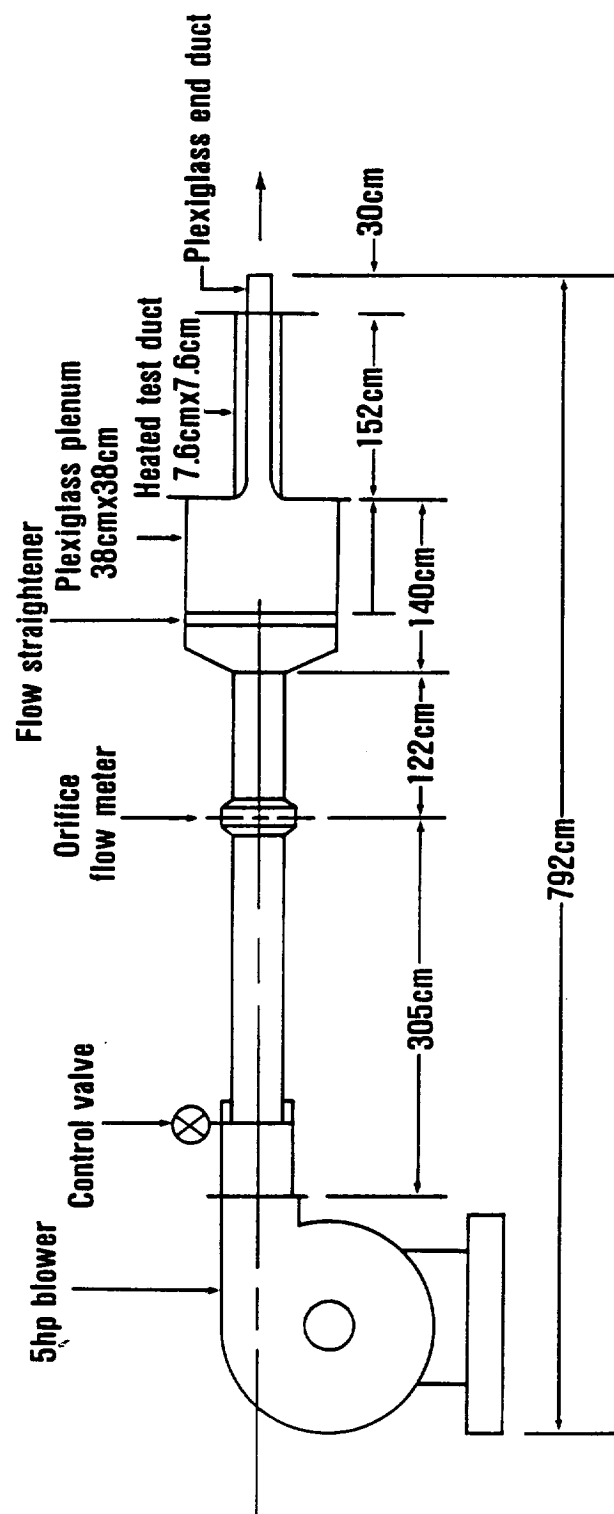


Figure 5. Test rig with sudden contraction entrance

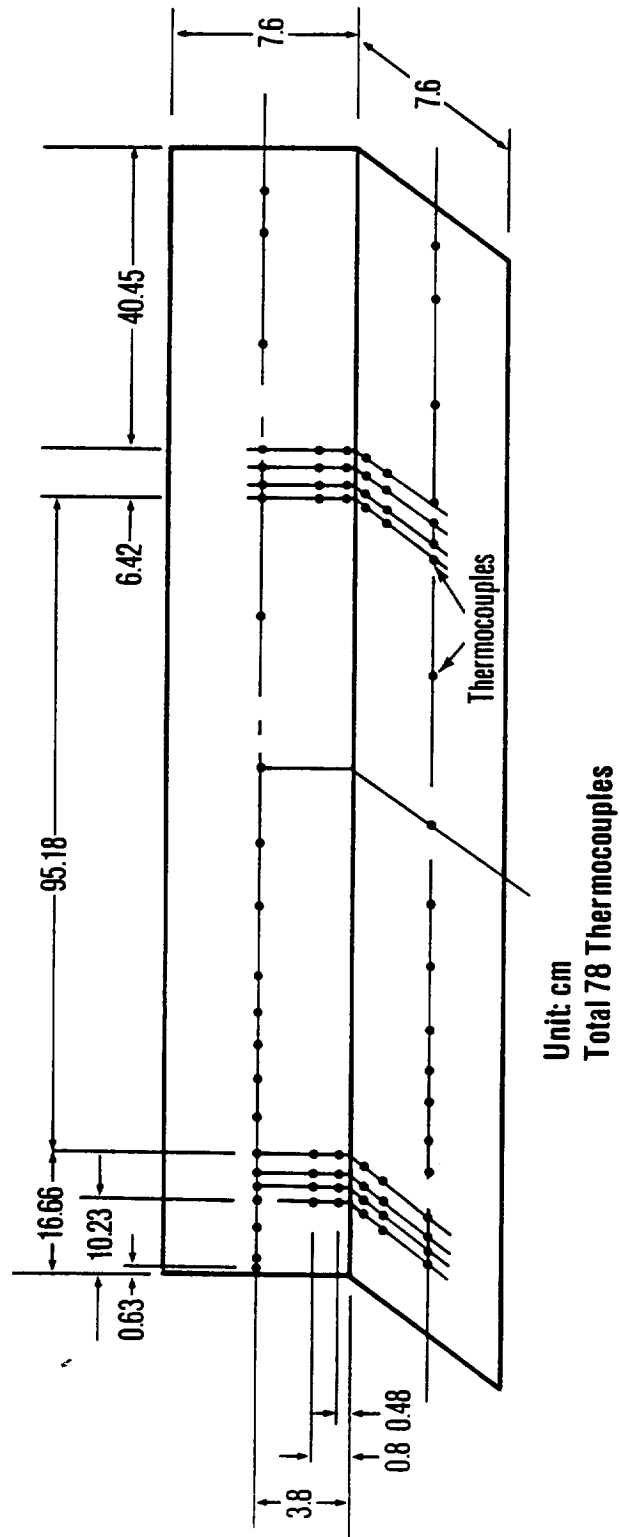


Figure 6. Detail of thermocouples distributions

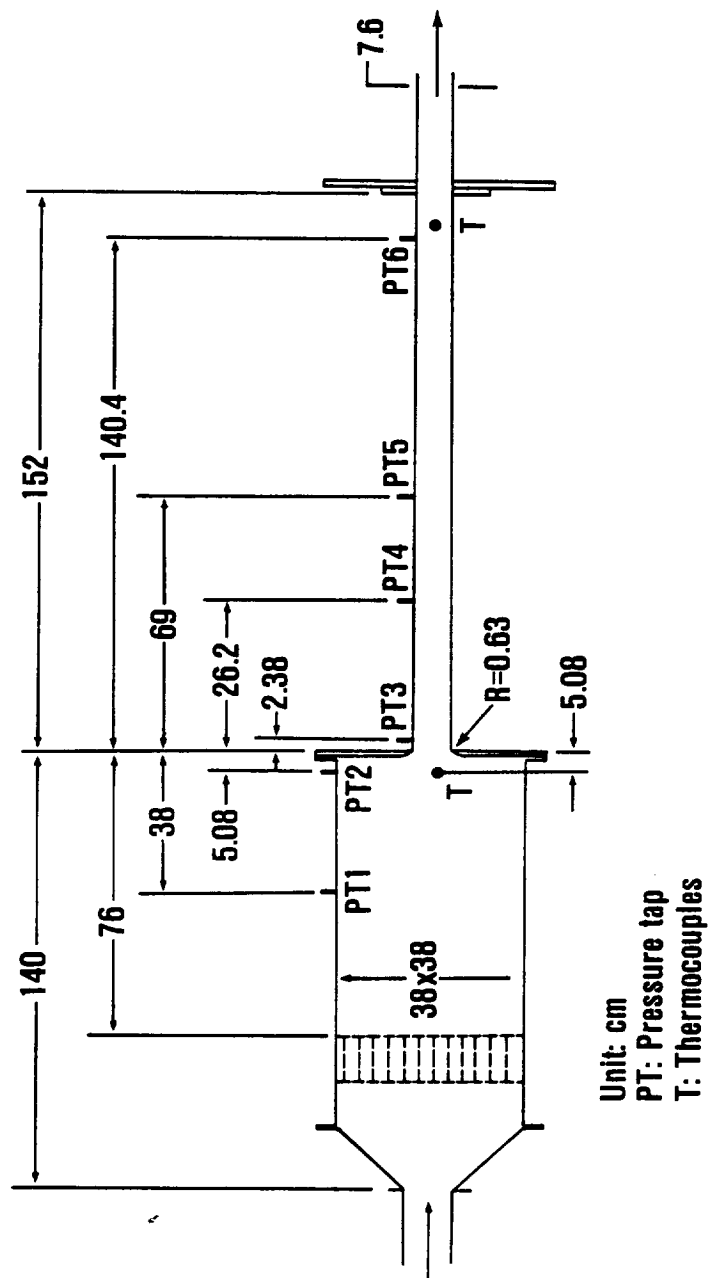


Figure 7. Detail of pressure taps locations

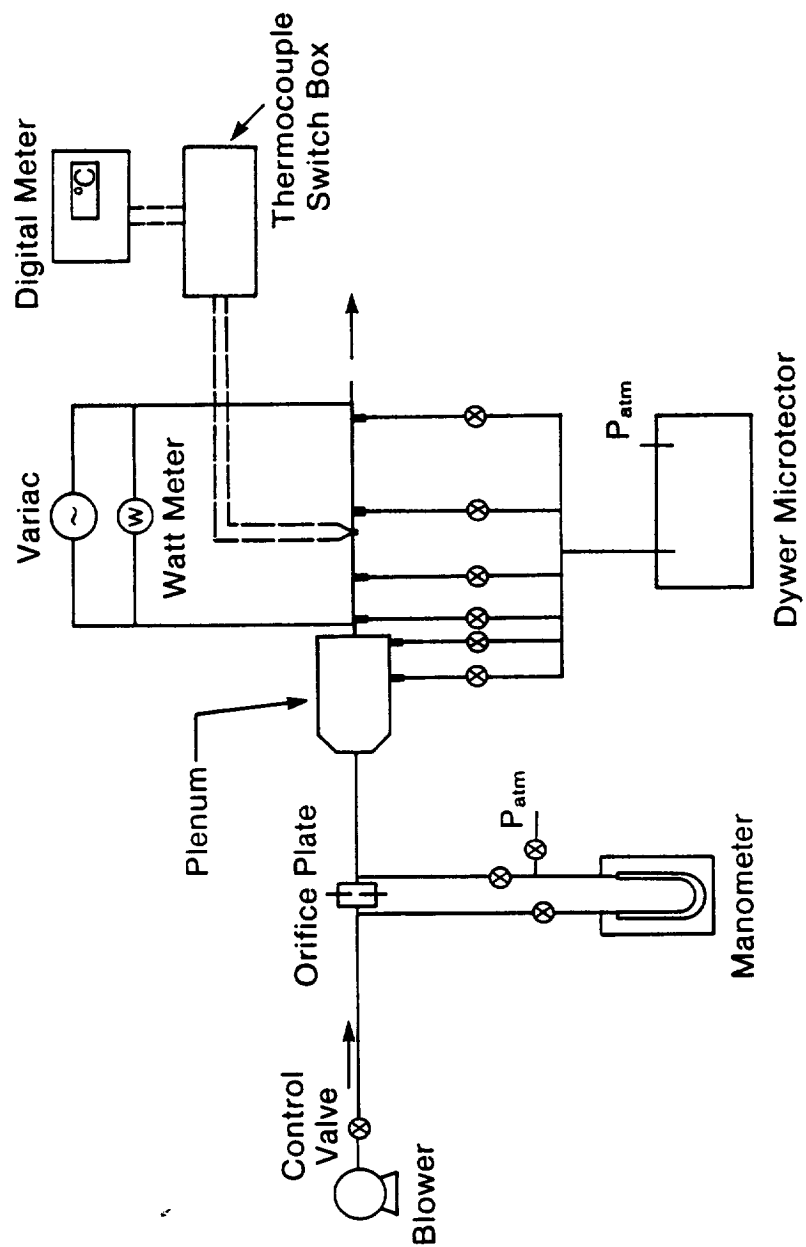


Figure 8. Flow, pressure drop, heat input, and temperature measurement systems

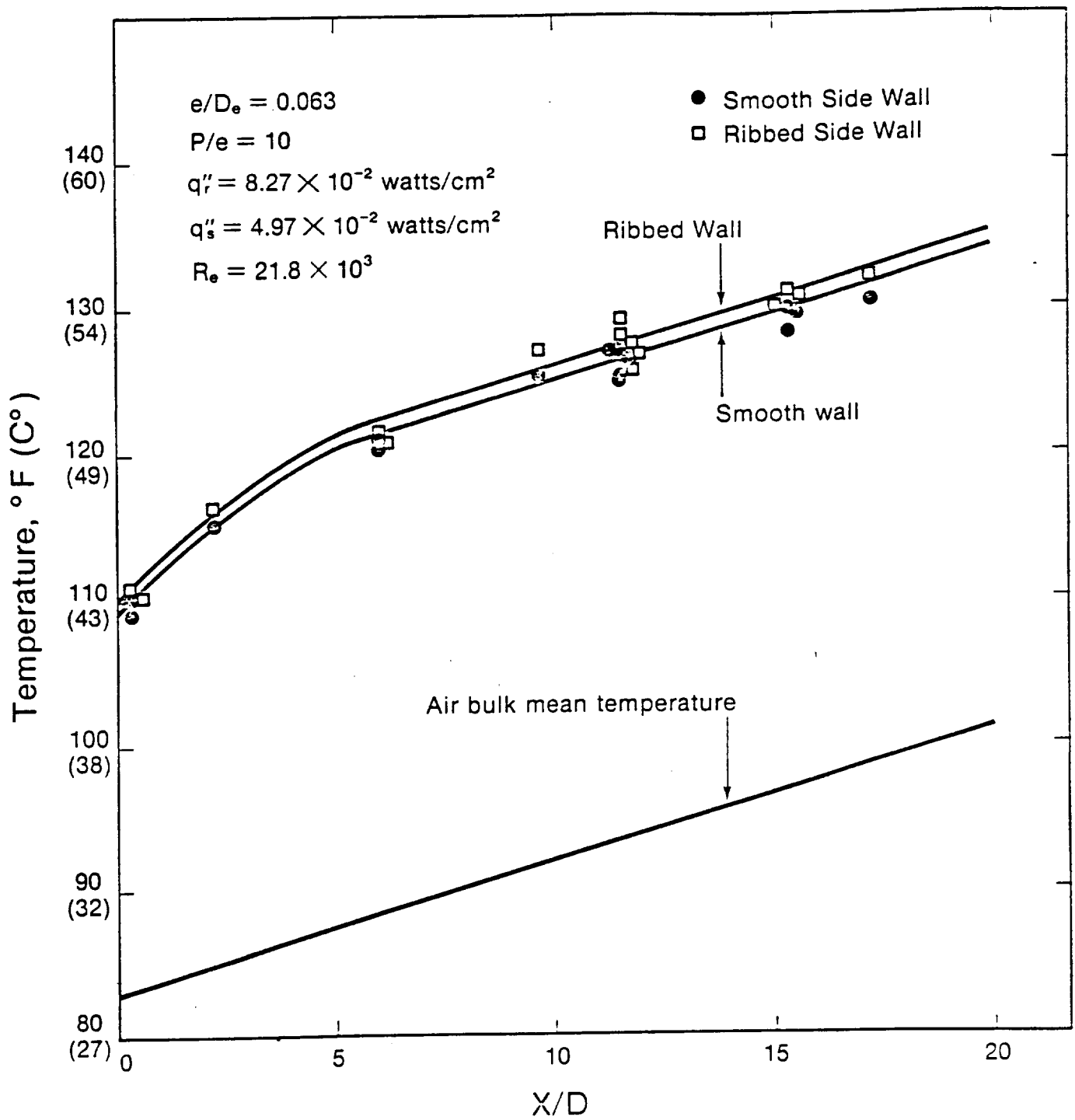


Figure 9. Air and wall temperature distributions along test duct

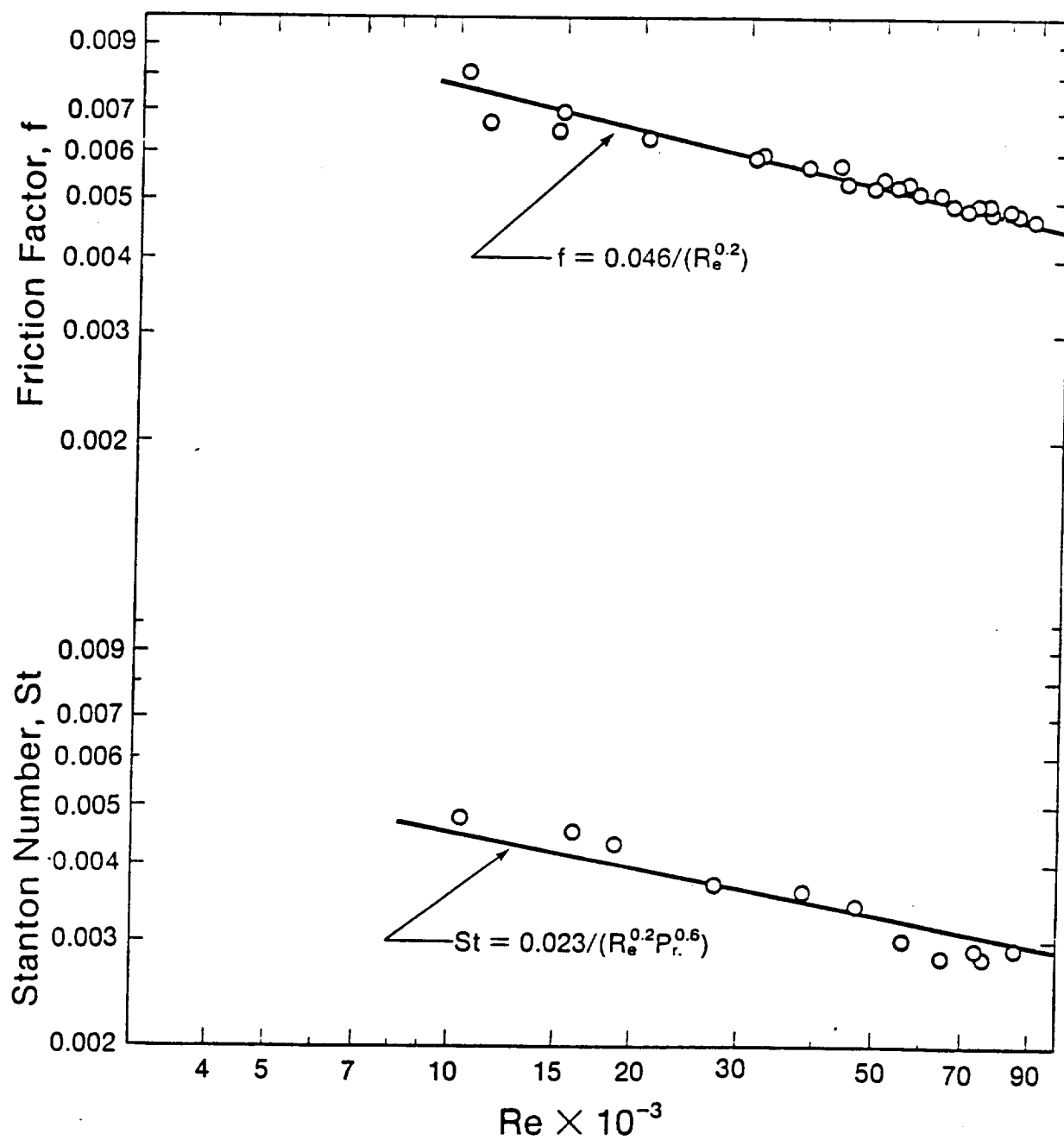


Figure 10. Test results for smooth surface

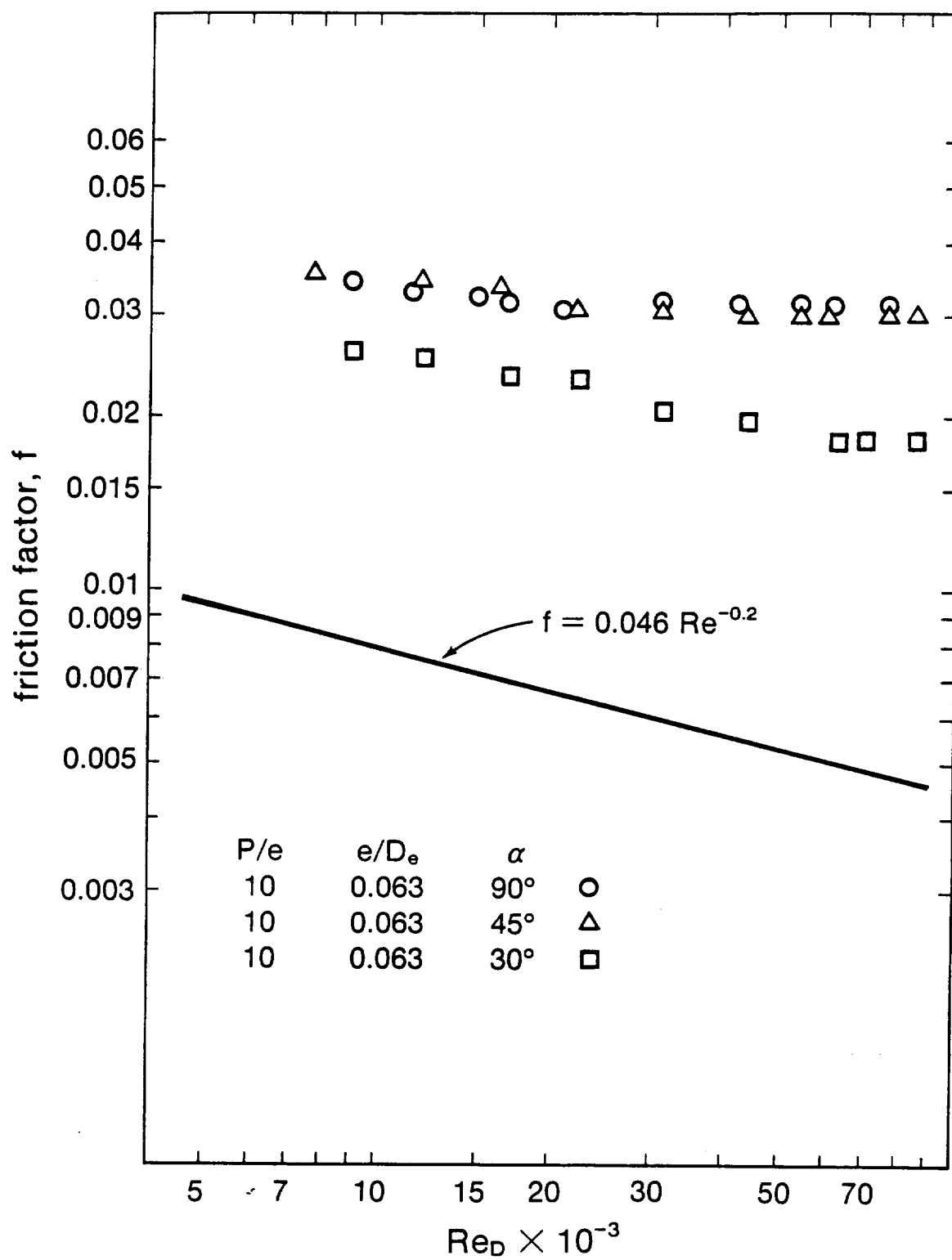


Figure 11. Friction factor vs Reynolds number at different rib angle-of-attack

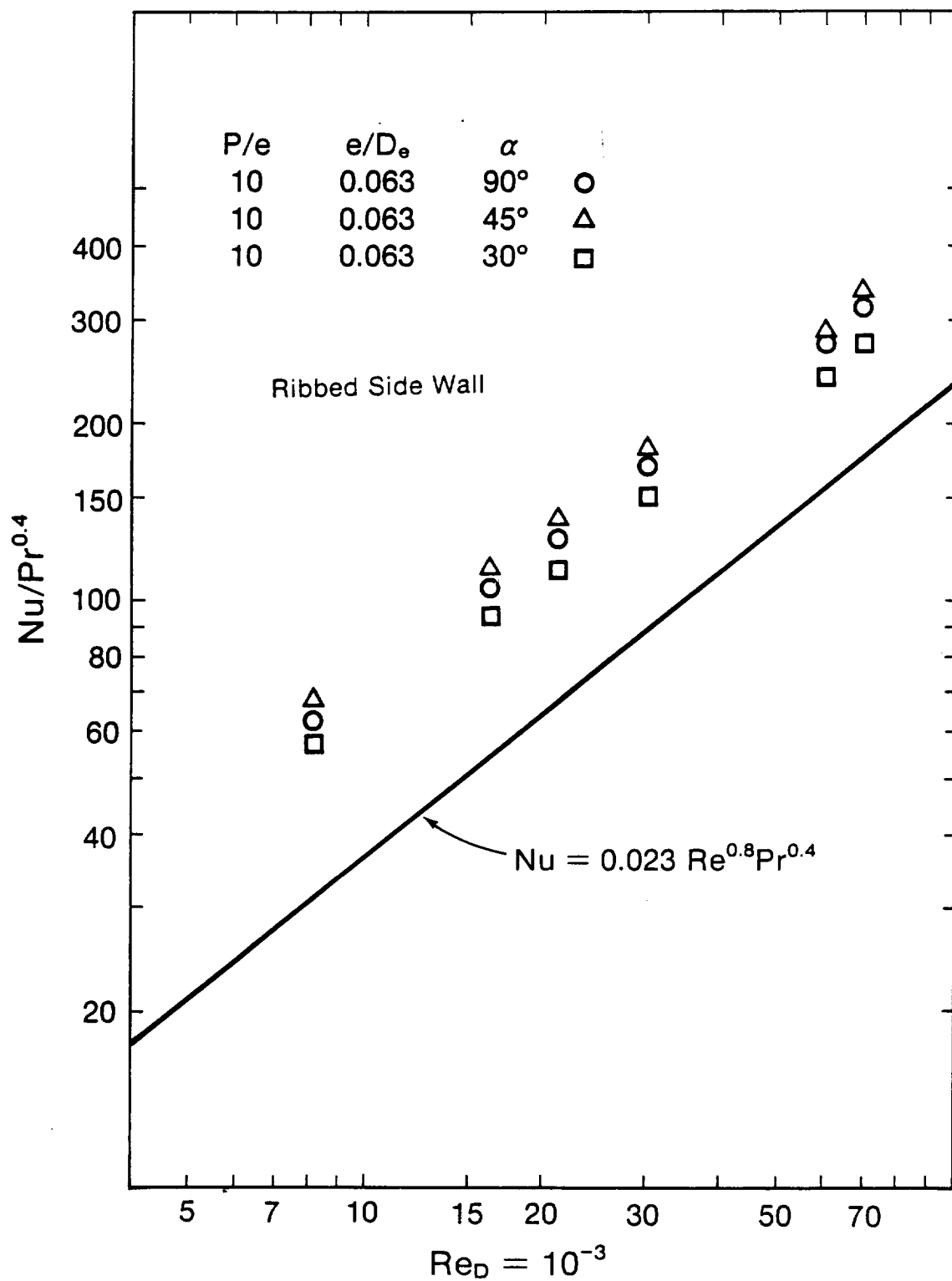


Figure 12. Nusselt number of ribbed side wall vs Reynolds number at different rib angle-of-attack

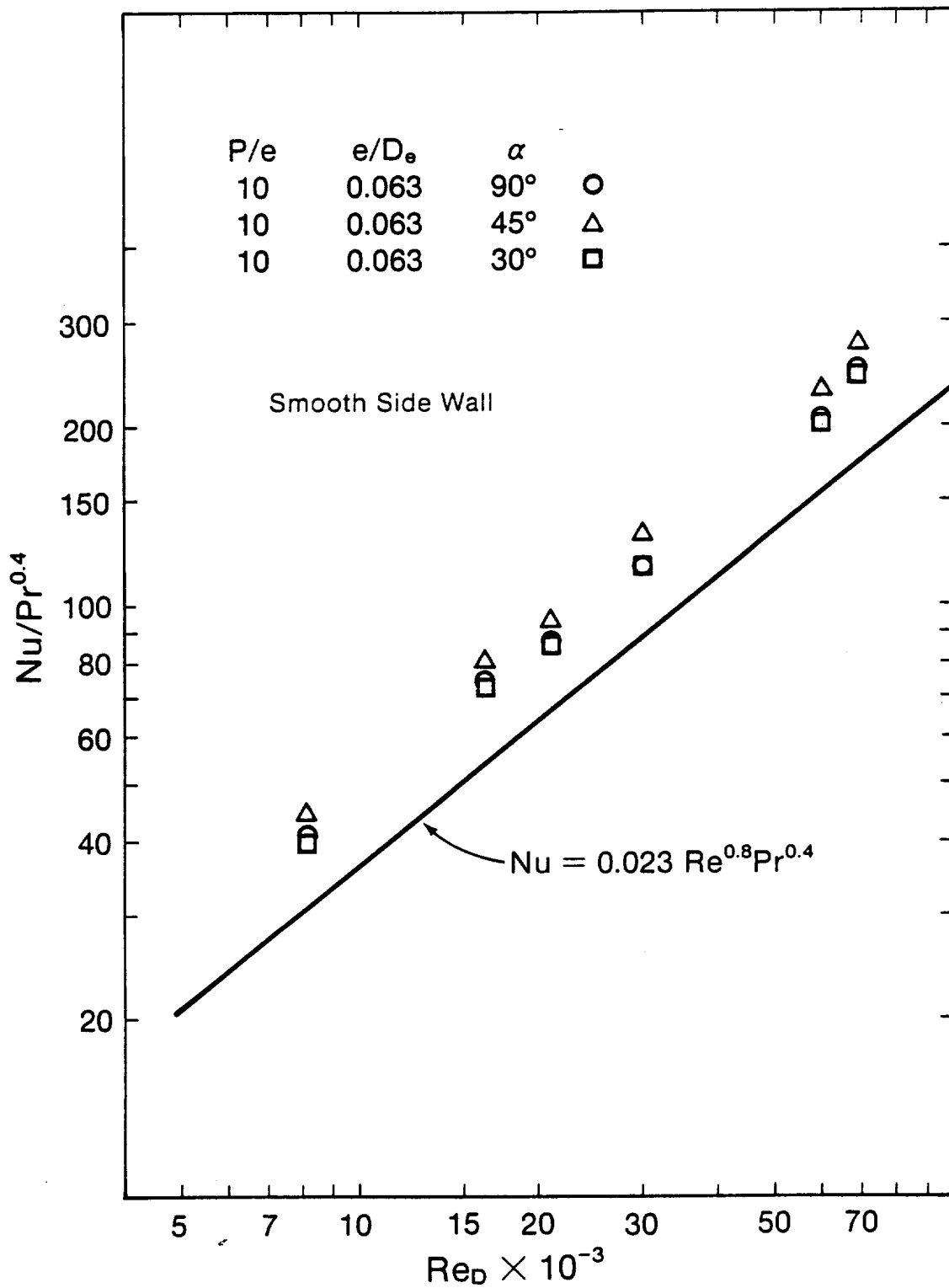


Figure 13. Nusselt number of smooth side wall vs Reynolds number at different rib angle-of-attack

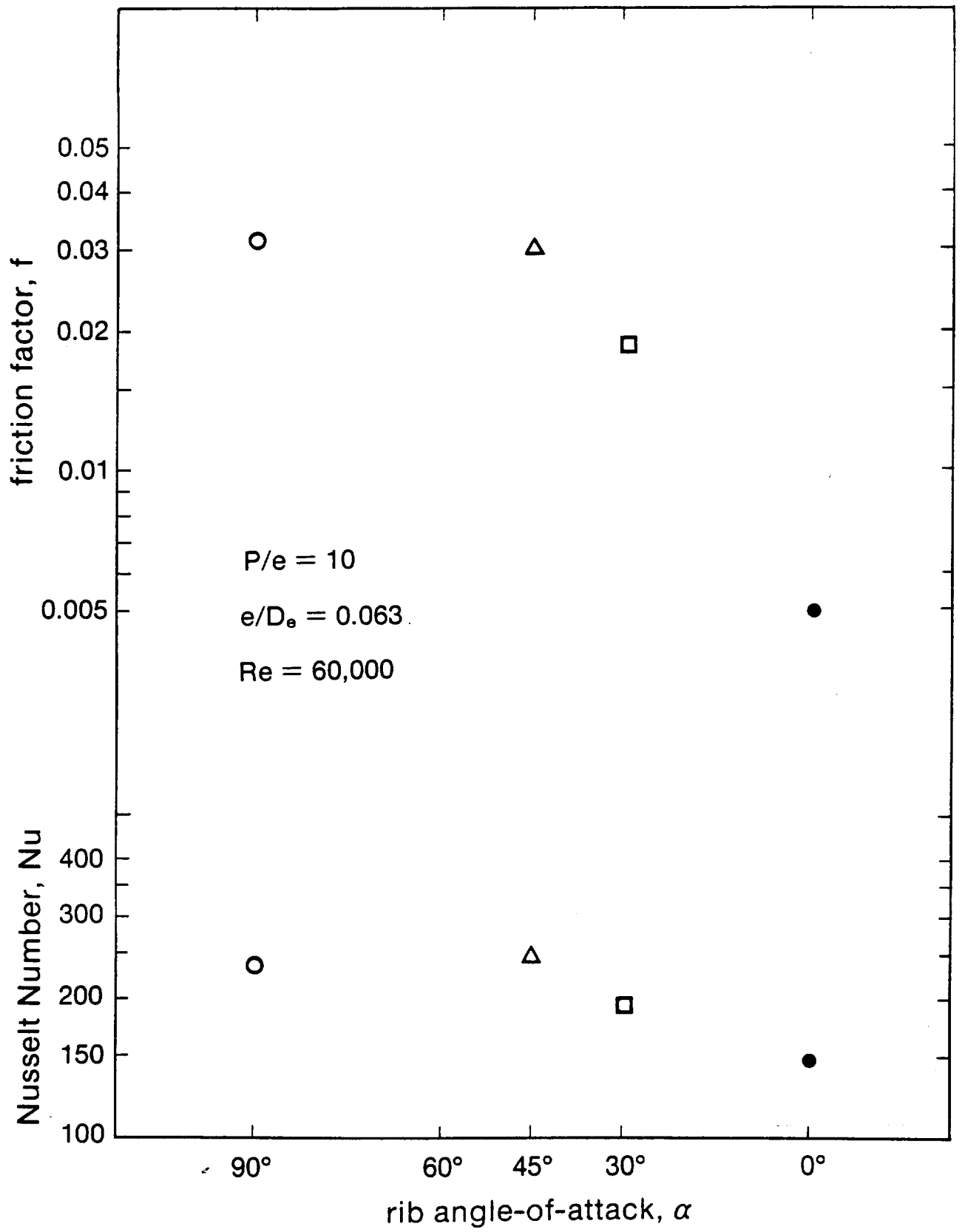


Figure 14. Friction factor and Nusselt number vs rib angle-of-attack

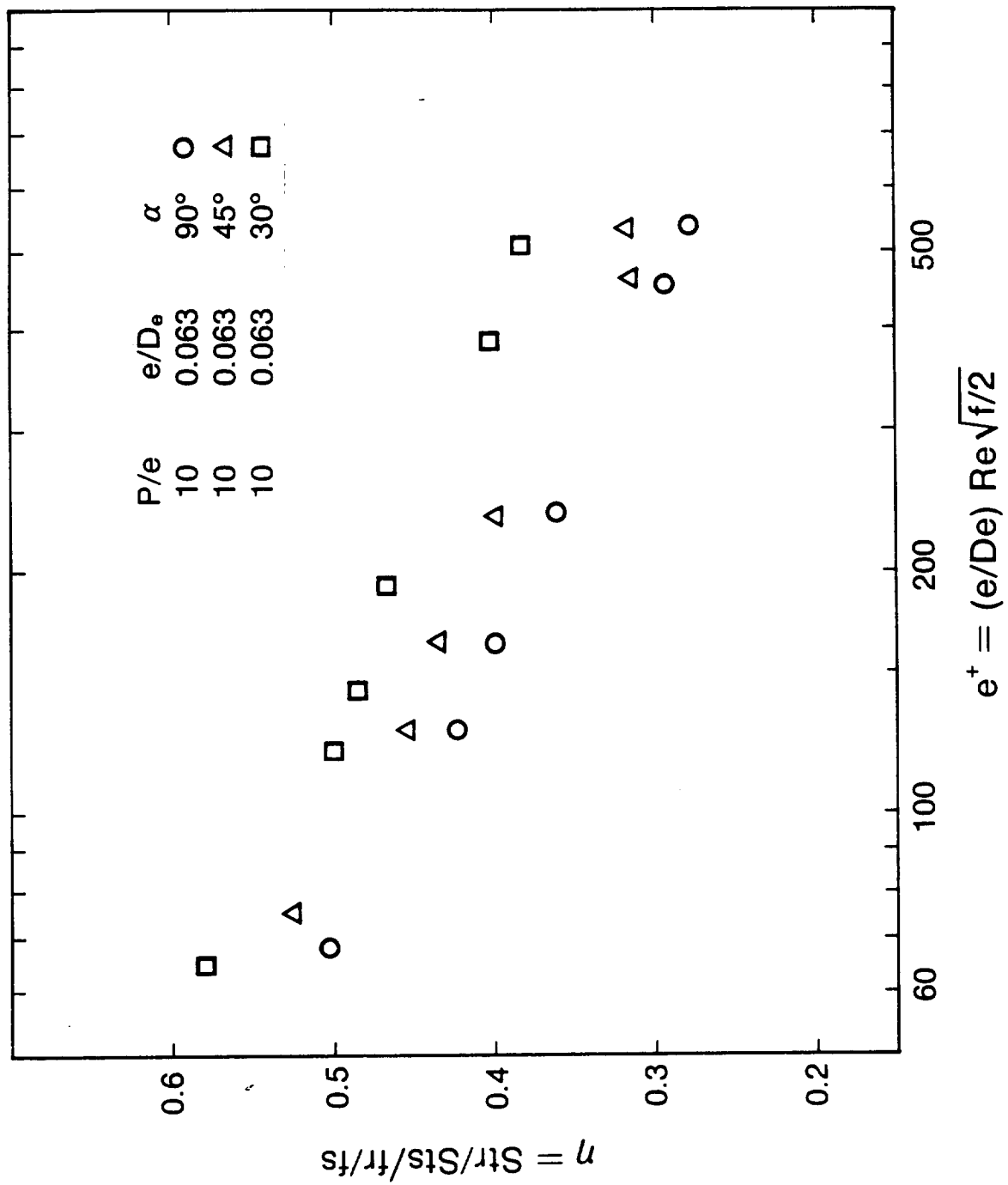


Figure 15. Efficiency index of ribbed duct vs roughness Reynolds number

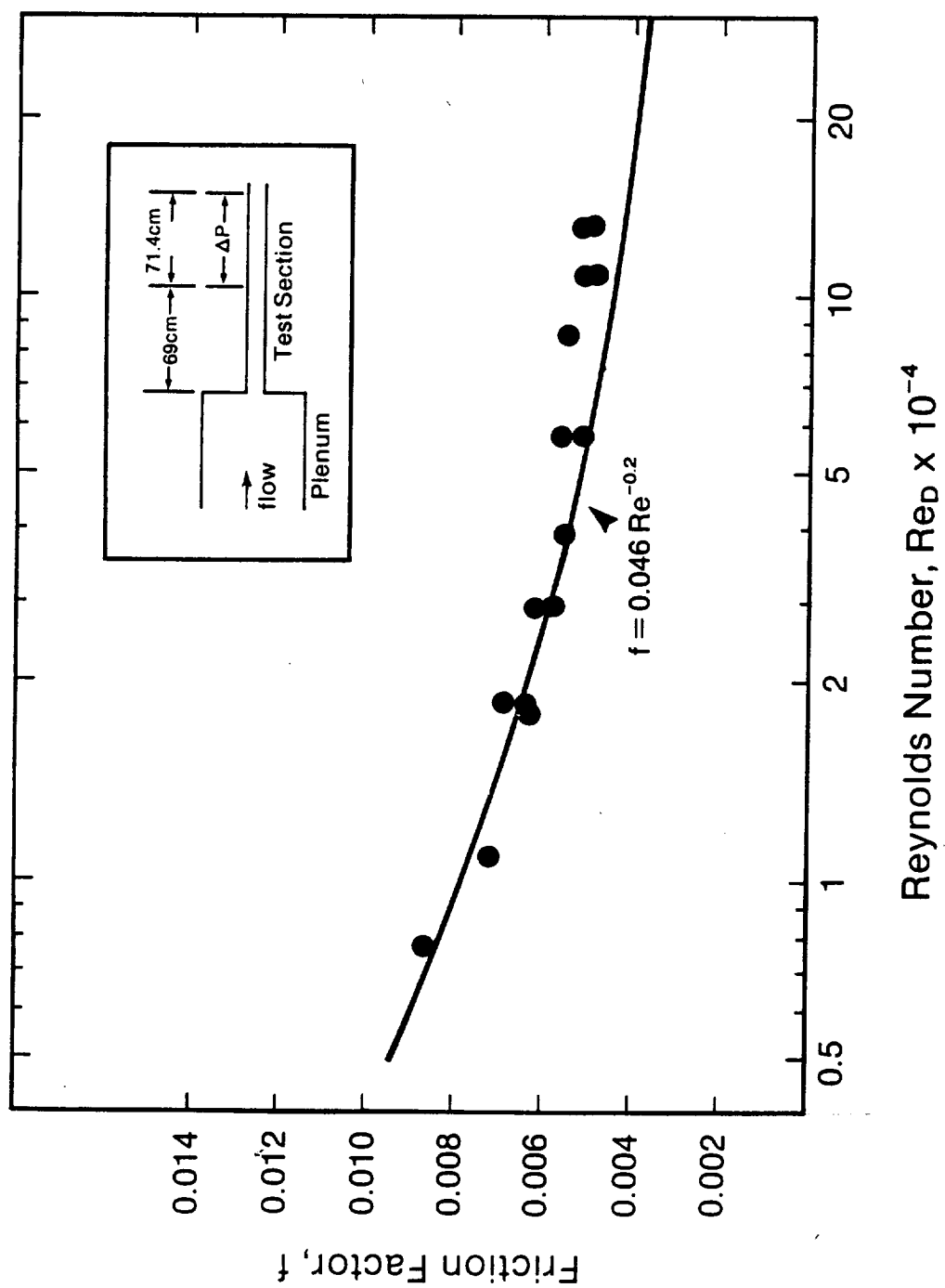


Figure 16. Friction factor vs Reynolds number for smooth duct

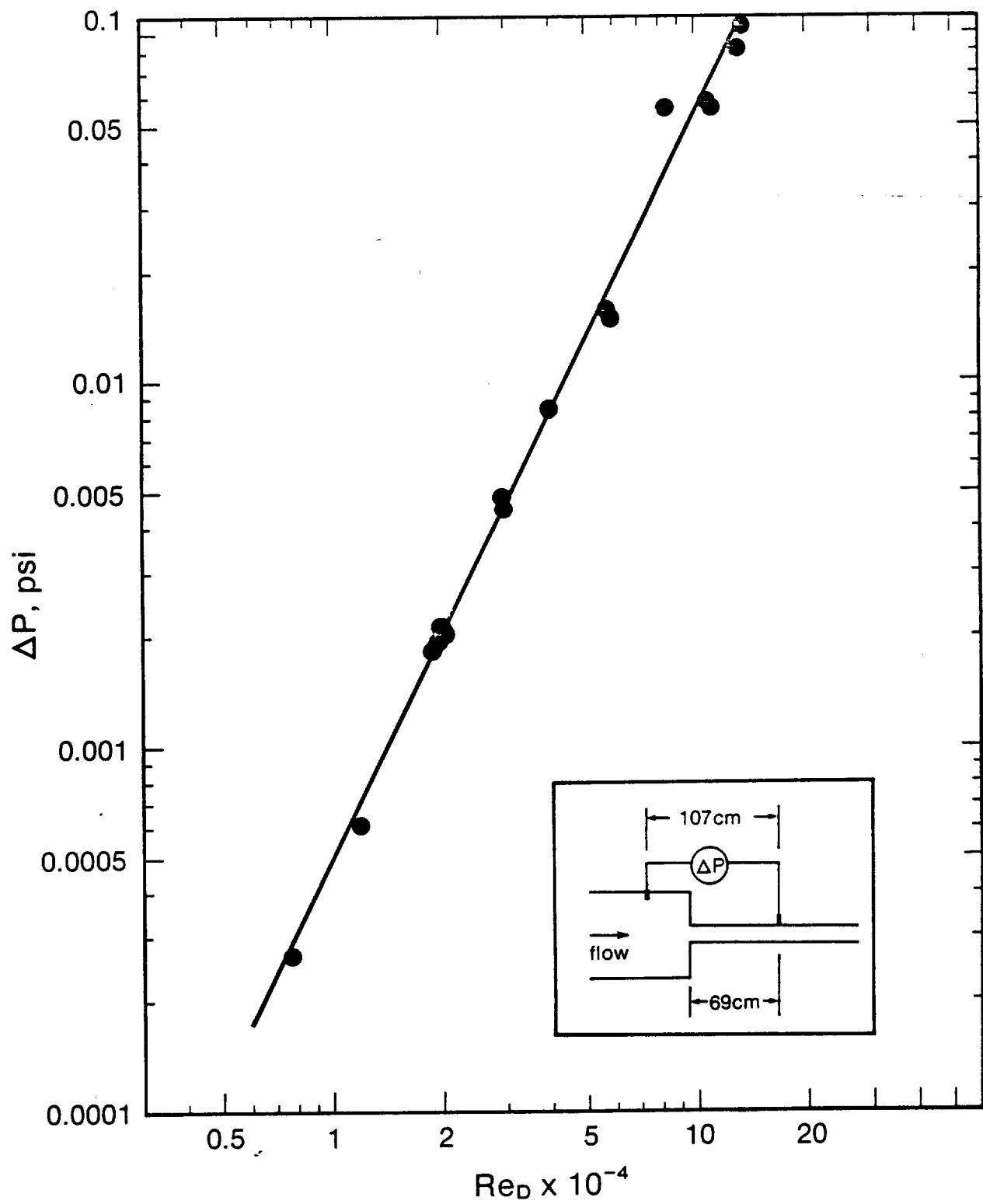


Figure 17. Plenum related pressure drop vs Reynolds number

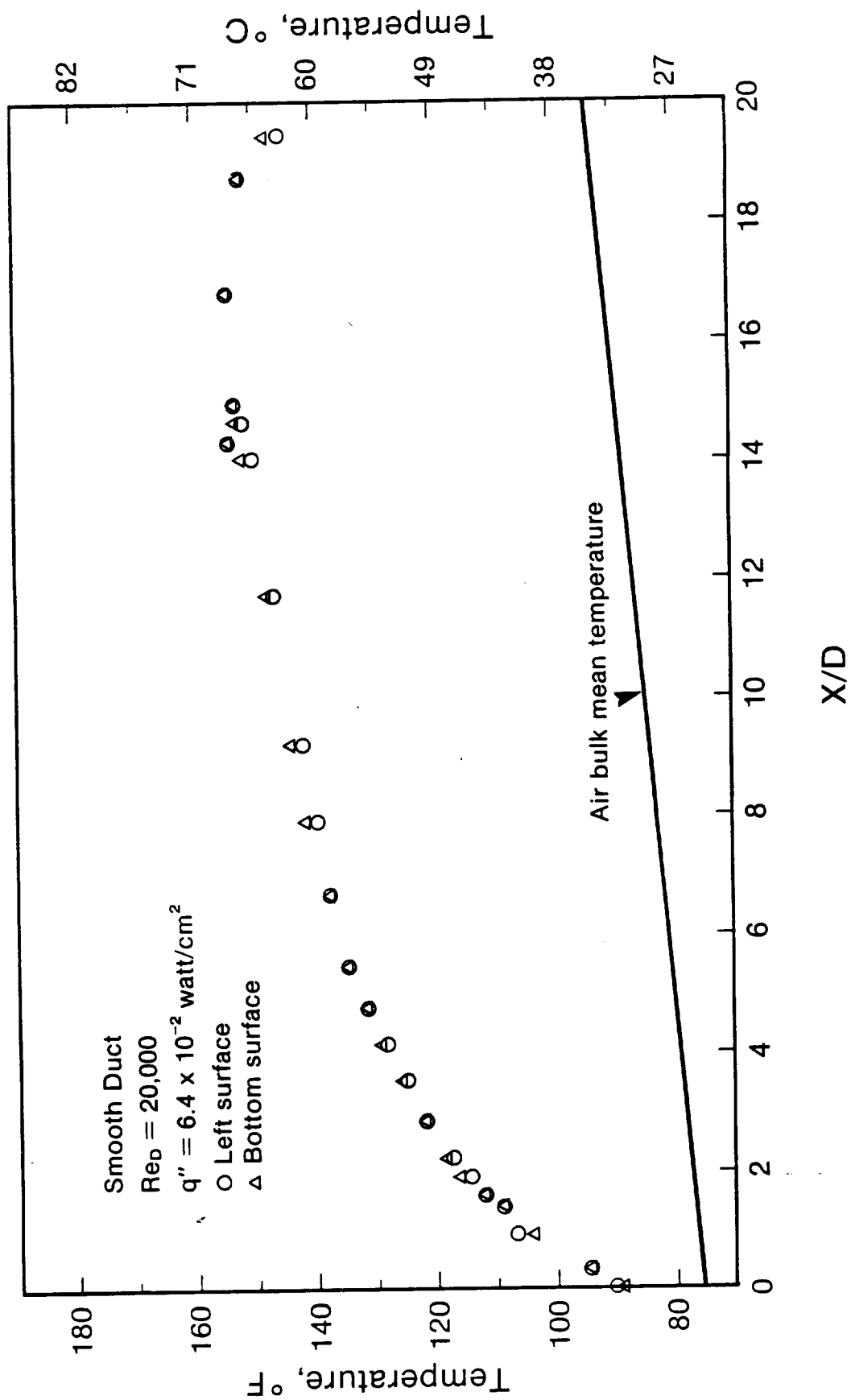


Figure 18. Temperature distributions along the test section at $Re_D = 20,000$

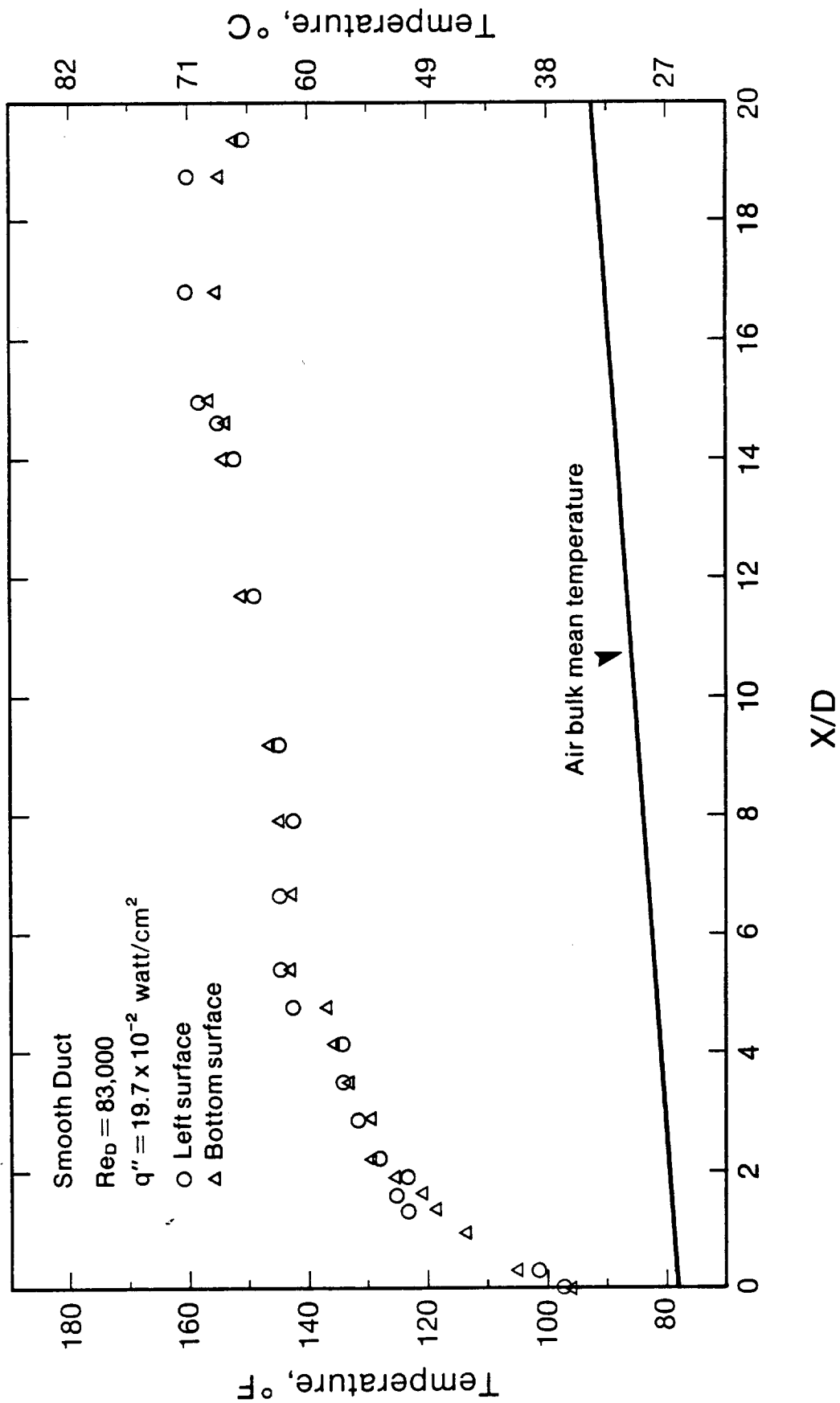


Figure 19. Temperature distributions along the test section at $Re_D = 83,000$

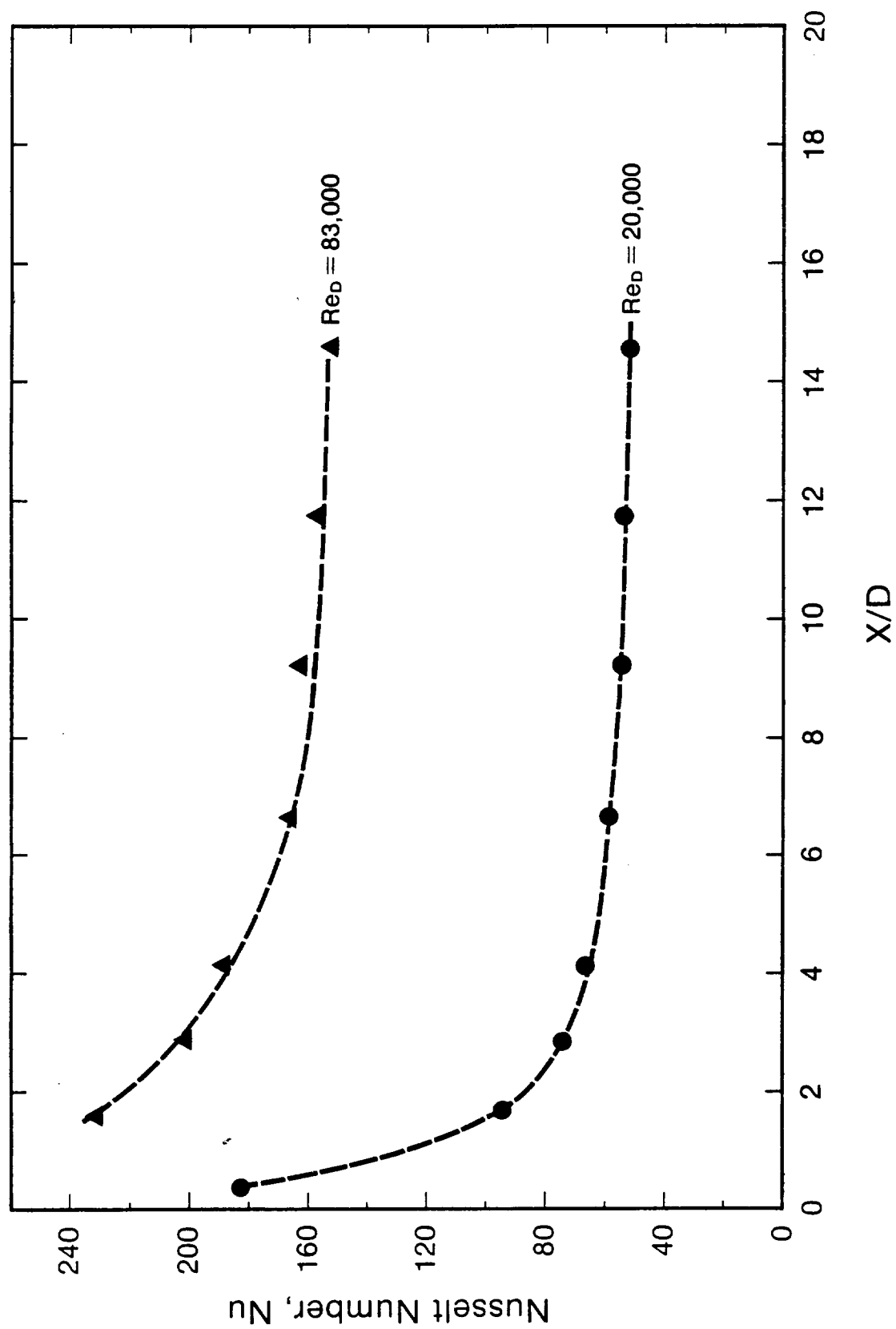


Figure 20. Local Nusselt number along the test section

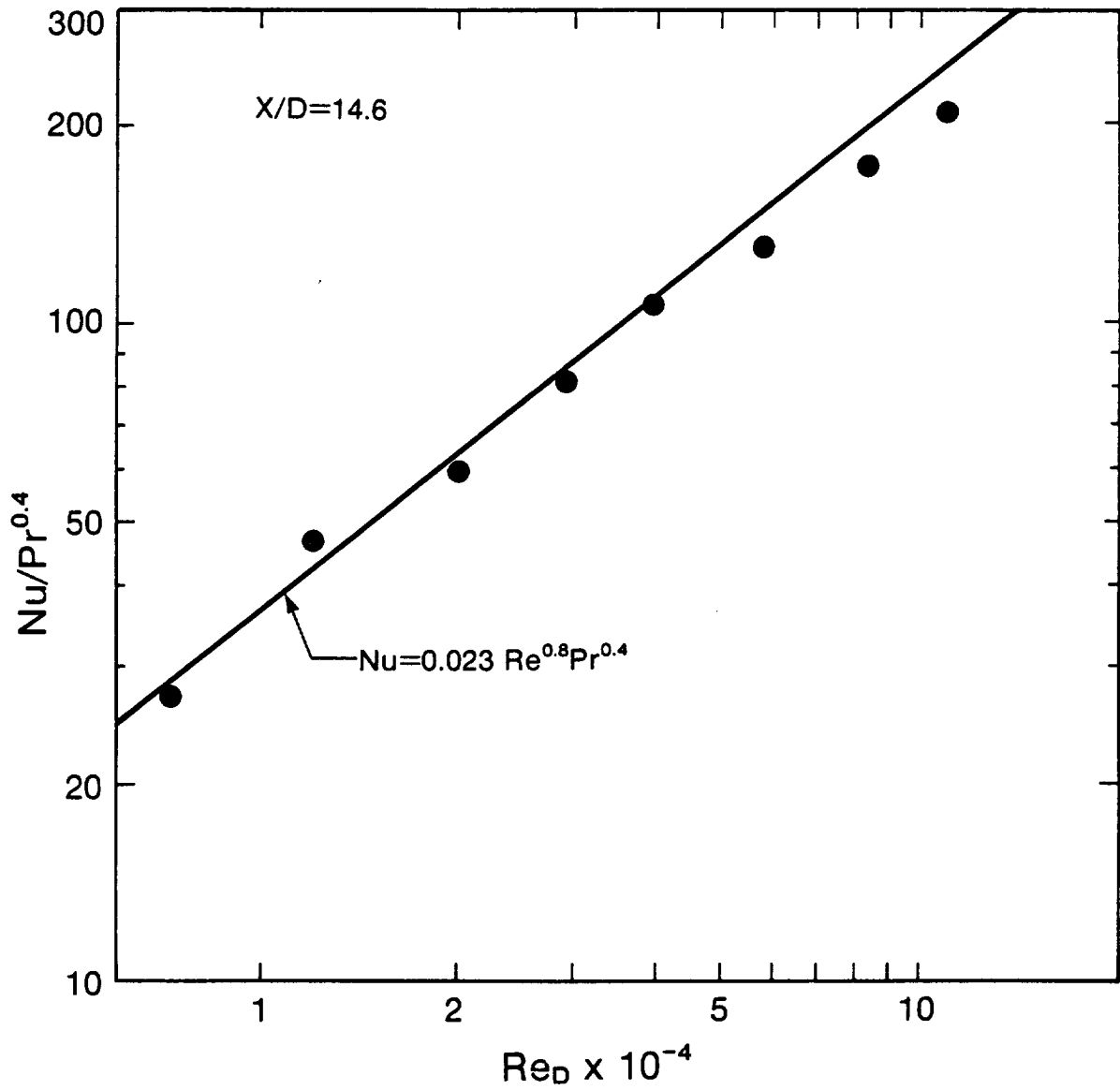


Figure 21. Nusselt number vs Reynolds number for smooth duct

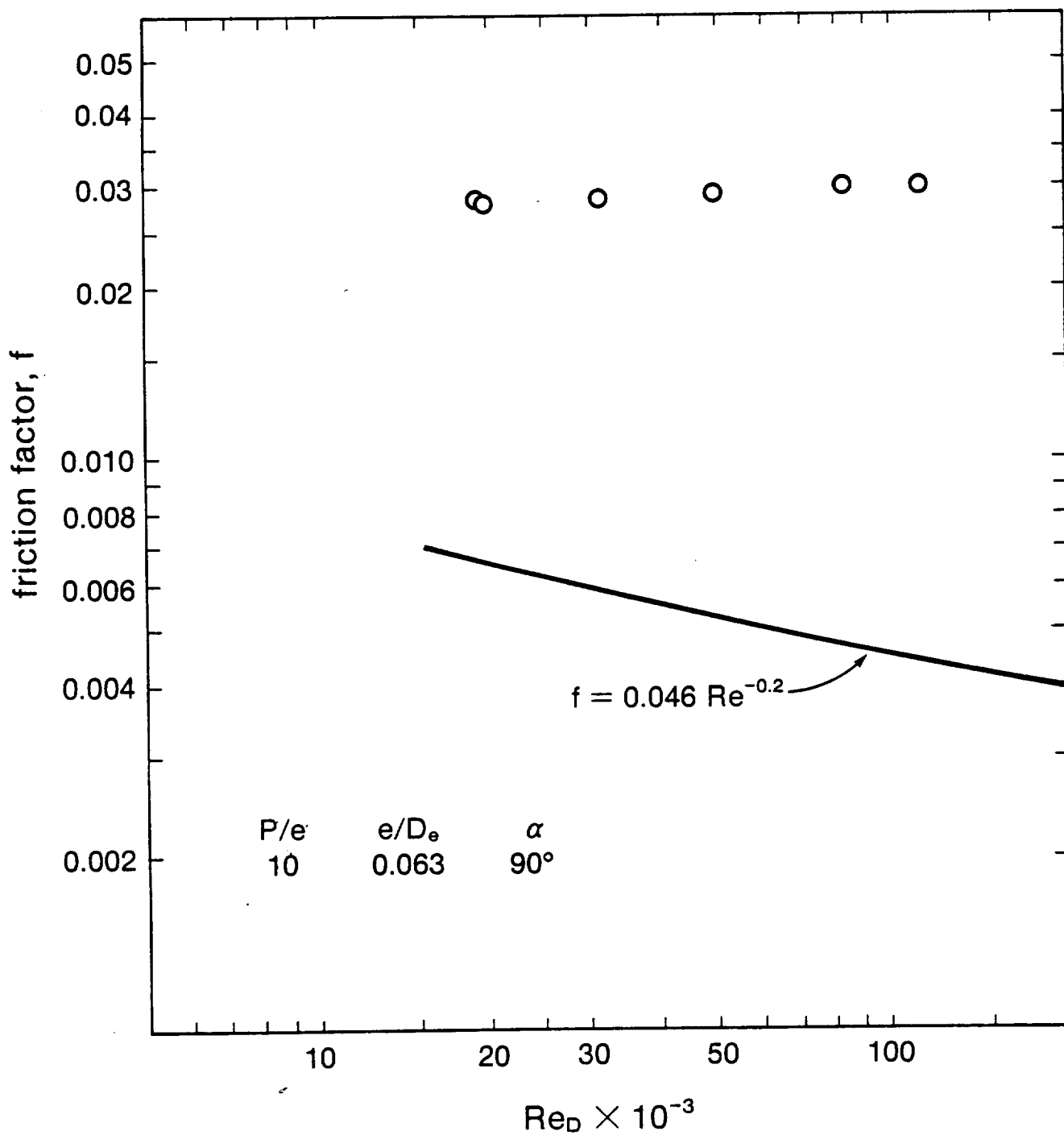


Figure 22. Friction factor vs Reynolds number

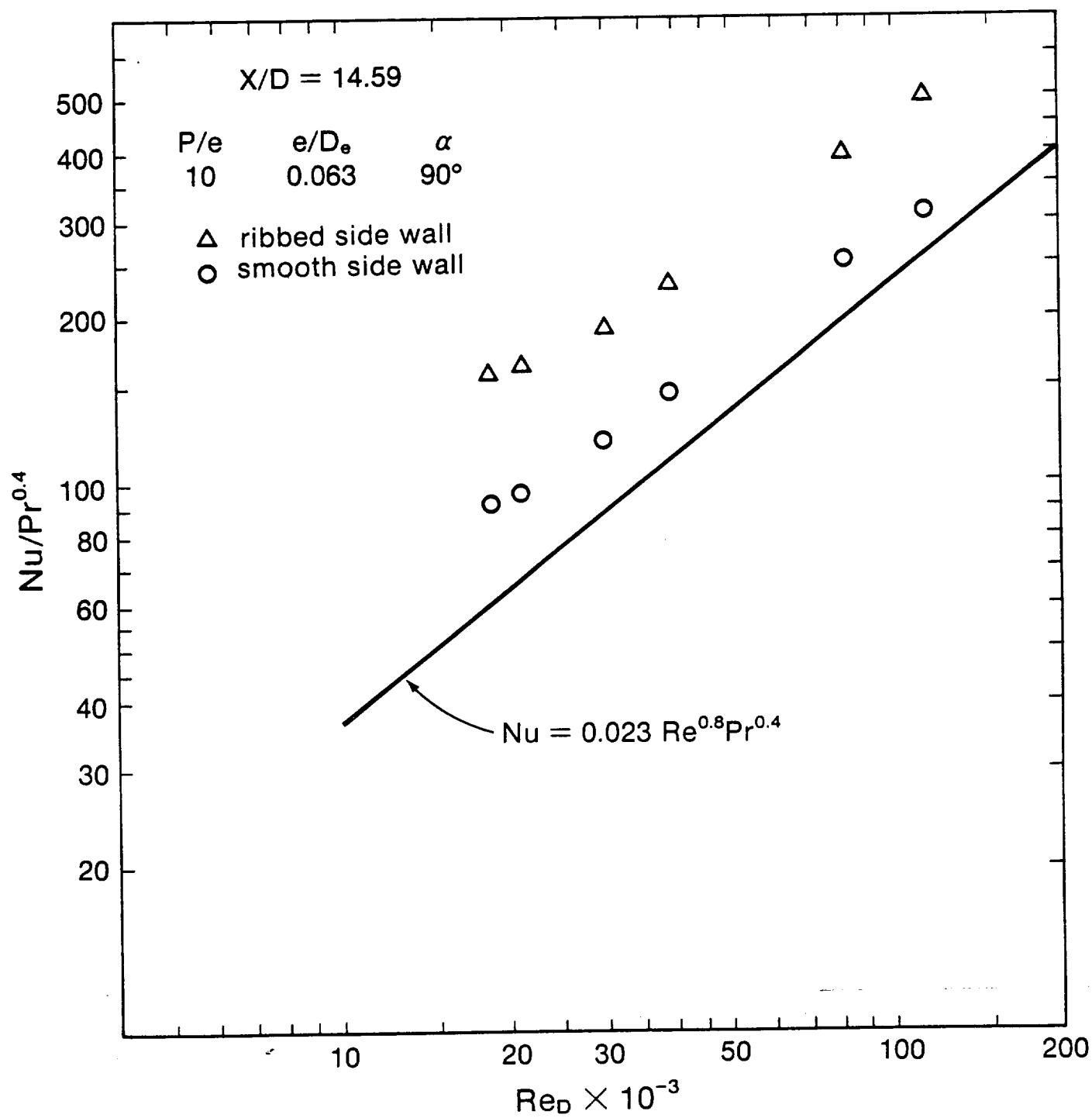
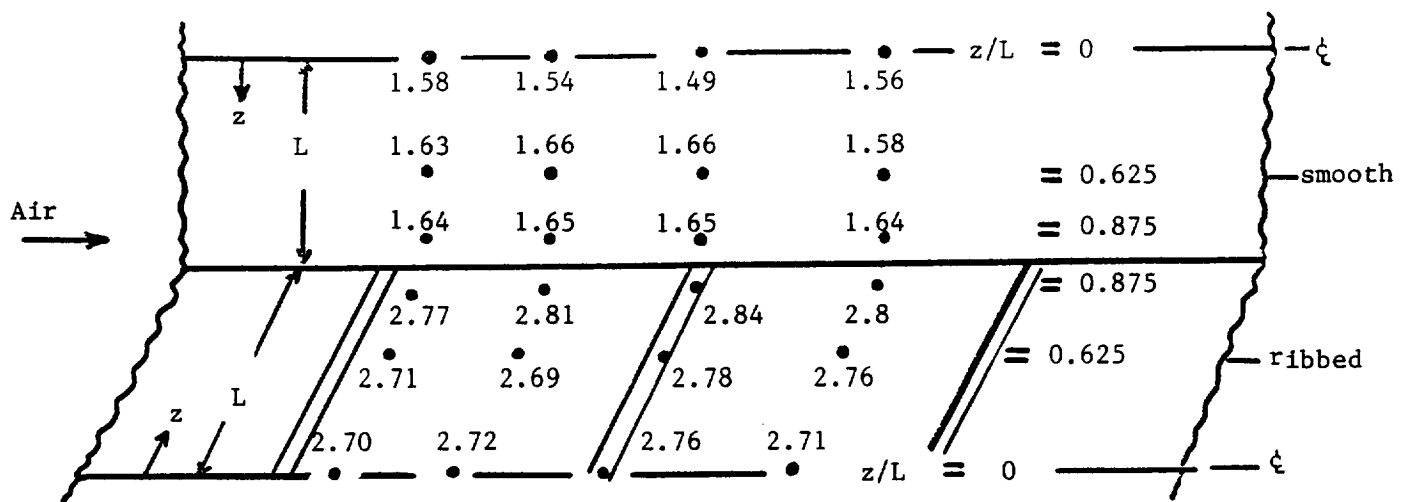


Figure 23. Nusselt number vs Reynold number



$$\frac{N_u}{N_{ufs}} = \frac{\text{Local Nusselt number}}{\text{Nusselt number of four sided smooth surfaces}}$$

$$Re_D = 20,000 \quad (\text{upper diagram})$$

$$Re_D = 80,000 \quad (\text{lower diagram})$$

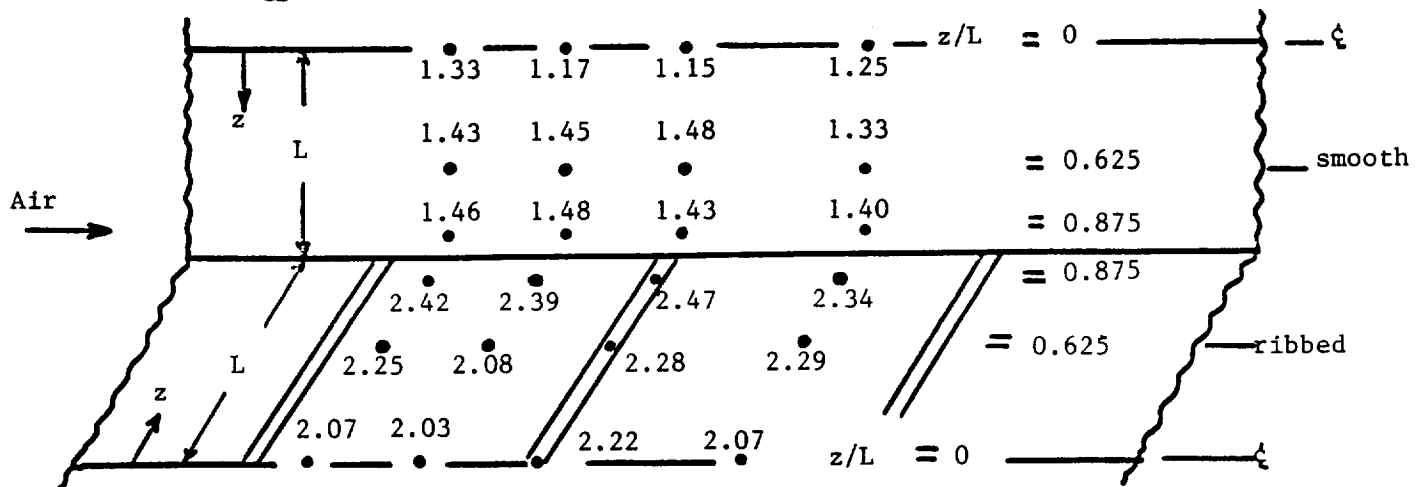


Figure 24. Local Nusselt number augmentation at the fully developed region for $p/e = 10$, $e/D_e = 0.063$, $\alpha = 90^\circ$

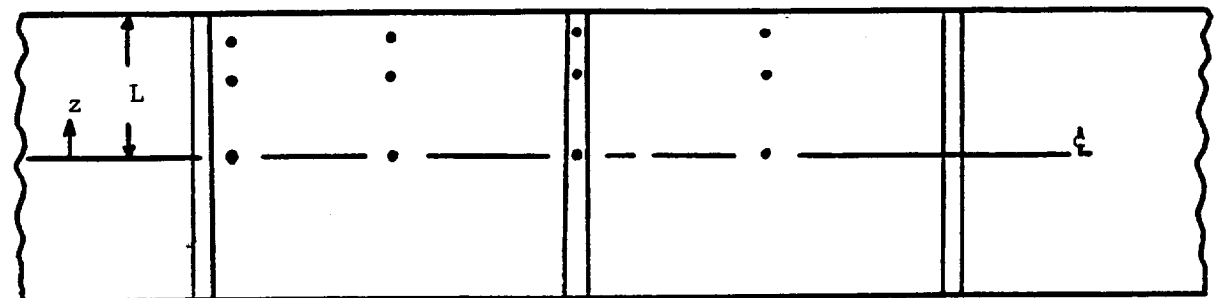
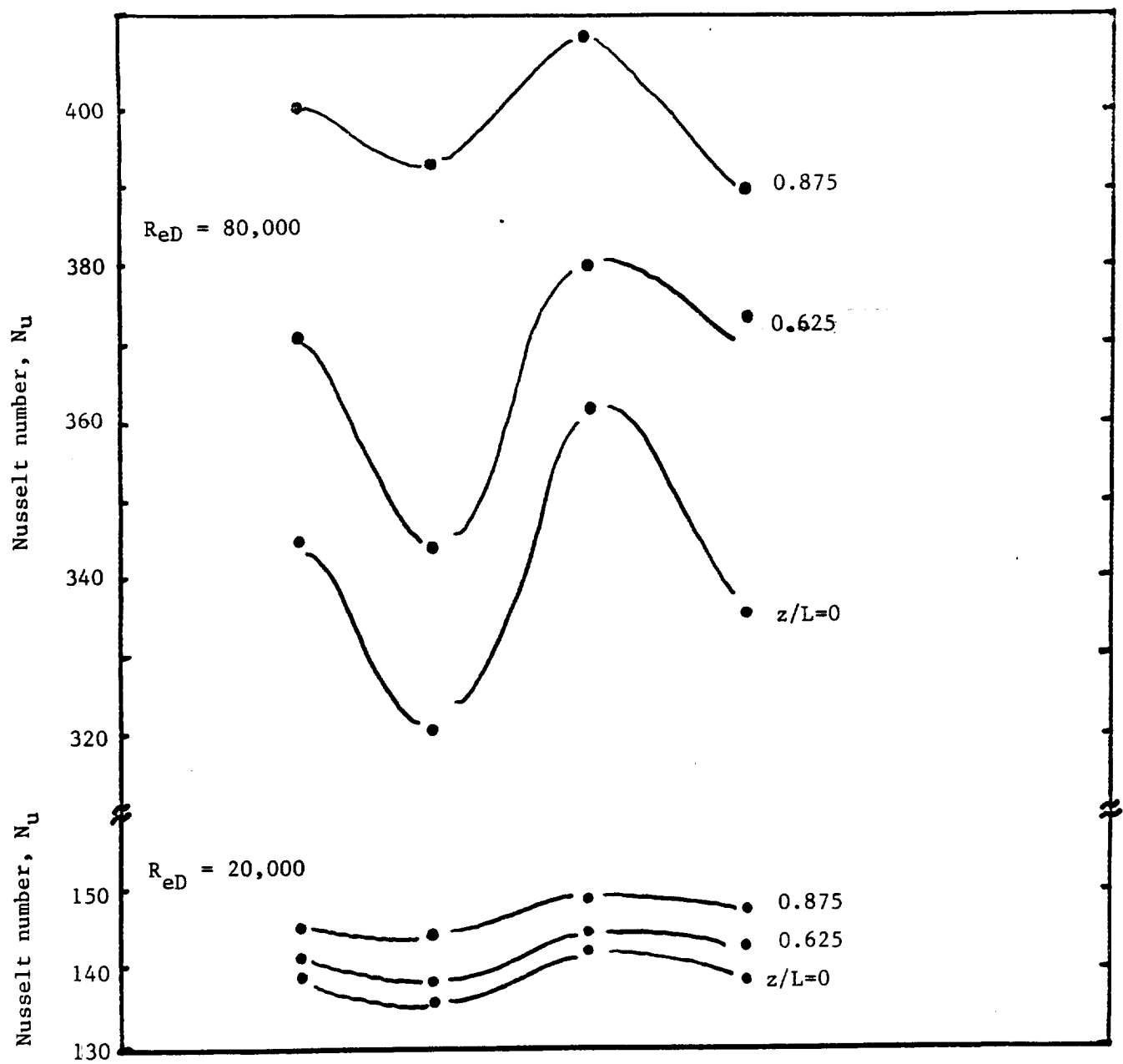
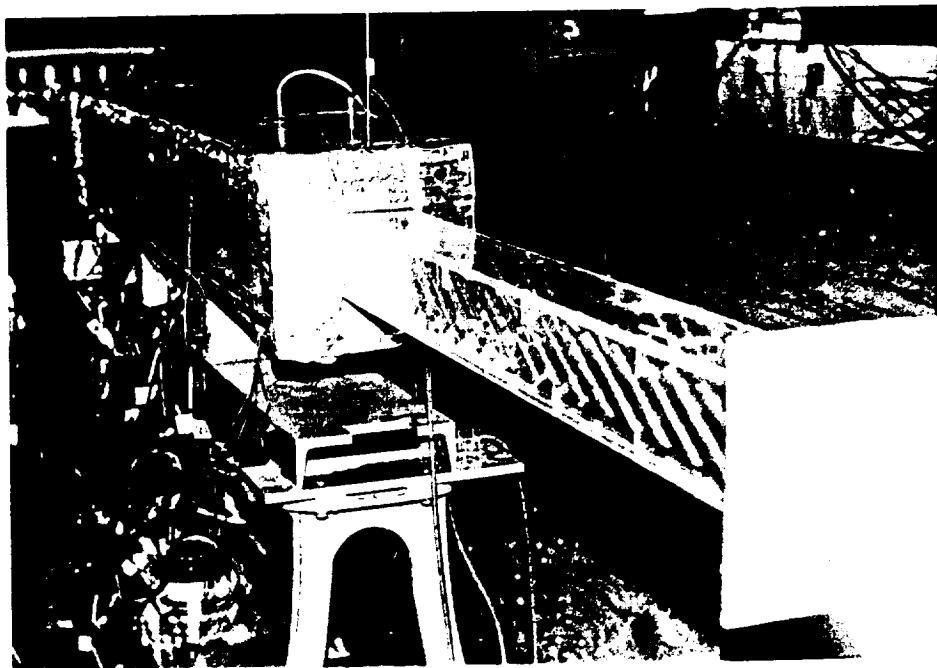
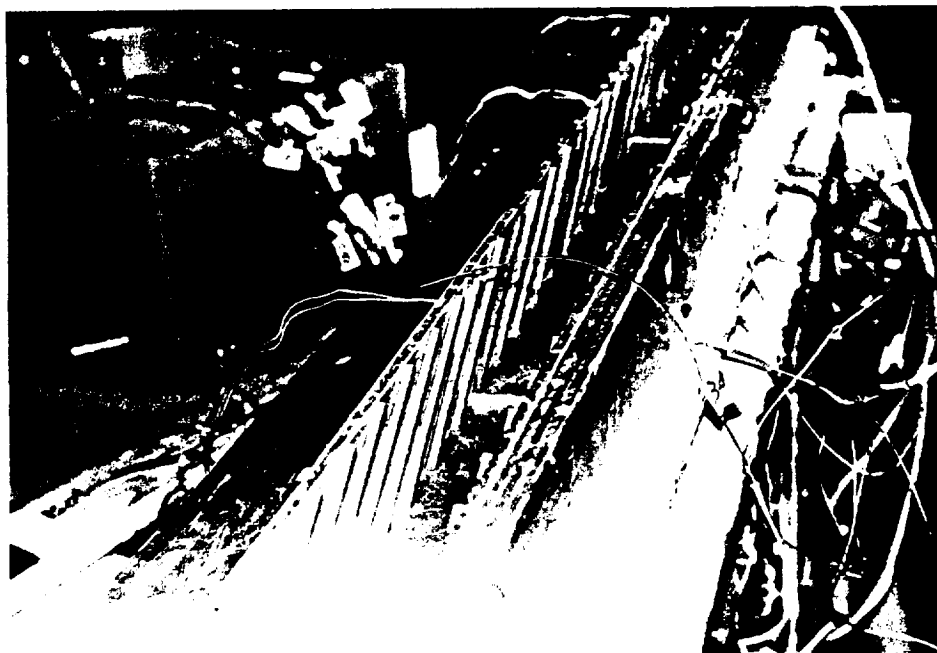


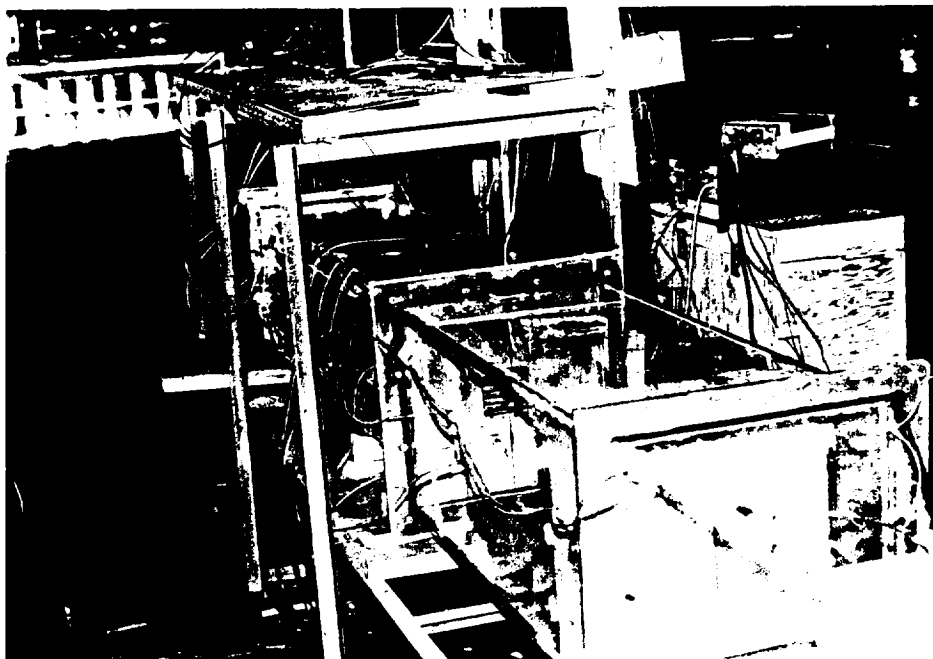
Figure 25. Local Nusselt number distribution between the ribs at the fully developed region for $p/e = 10$, $e/D_e = 0.063$, $\alpha = 90^\circ$



Upper photo: Test rig with long duct entrance

Lower photo: Opposite ribs at $\alpha = 30^\circ$





Upper photo: Test rig with sudden contraction entrance

Lower photo: Instrumentations and measurements facilities

